

Four Generations of Quantum Biomedical Sensors

Xin Jin,^{1,*} Priyam Srivastava,^{2,*} Ronghe Wang,³ Yuqing Li,¹ Jonathan Beaumariage,³ Tom Purdy,³ M. V. Gurudev Dutt,³ Kang Kim,^{4,5} Kaushik Seshadreesan,^{2,3} and Junyu Liu^{1,†}

¹*Department of Computer Science, University of Pittsburgh, Pittsburgh, PA 15260, USA*

²*Department of Informatics and Networked Systems, University of Pittsburgh, Pittsburgh, PA 15260, USA*

³*Department of Physics and Astronomy, University of Pittsburgh, Pittsburgh, PA 15260, USA*

⁴*Department of Medicine, University of Pittsburgh School of Medicine, Pittsburgh, PA 15213, USA*

⁵*Department of Bioengineering, University of Pittsburgh, Pittsburgh, PA 15261, USA*

(Dated: April 1, 2026)

Quantum sensing technologies offer transformative potential for ultra-sensitive biomedical sensing, yet their clinical translation remains constrained by classical noise limits and a reliance on macroscopic ensembles. We propose a unifying generational framework to organize the evolving landscape of quantum biosensors based on their utilization of quantum resources. First-generation devices utilize discrete energy levels for signal transduction but follow classical scaling laws. Second-generation sensors exploit quantum coherence to reach the standard quantum limit, while third-generation architectures leverage entanglement and spin squeezing to approach Heisenberg-limited precision. We further define an emerging fourth generation characterized by the end-to-end integration of quantum sensing with quantum learning and variational circuits, enabling adaptive inference directly within the quantum domain. By analyzing critical parameters such as bandwidth matching and sensor-tissue proximity, we identify key technological bottlenecks and propose a roadmap for transitioning from measuring physical observables to extracting structured biological information with quantum-enhanced intelligence.

I. INTRODUCTION

Quantum sensing has emerged as a transformative paradigm in measurement science, exploiting the fundamental principles of quantum mechanics to detect physical quantities with unprecedented sensitivity and precision [1–4]. In contrast to conventional biomedical sensing, which relies on macroscopic transduction and ensemble-averaged signals limited by classical noise, quantum sensors encode physical parameters into quantum states whose evolution can be measured with enhanced precision [5]. By harnessing quantum superposition, coherence, and entanglement, quantum sensing enables detection of extremely weak magnetic and electric fields, temperature variations, pressure fluctuations, and chemical or molecular environments [6]. These capabilities allow sensitivities that surpass the standard quantum limit (SQL) and in principle approach the Heisenberg limit [7]. Classical biomedical sensors ultimately depend on quantum physics at the microscopic level, but they do not deliberately manipulate quantum resources such as coherence or entanglement. Quantum sensors, in contrast, explicitly engineer quantum states as metrological resources to enhance measurement precision.

The Importance of a Generational Framework. Rapid advances in biomedical quantum sensing have produced a diverse landscape of sensing platforms, including superconducting circuits, nitrogen-vacancy (NV) centers, atomic magnetometers, and entanglement-enhanced metrology. Despite this progress, the field lacks a systematic framework for comparing sensing architectures according to the

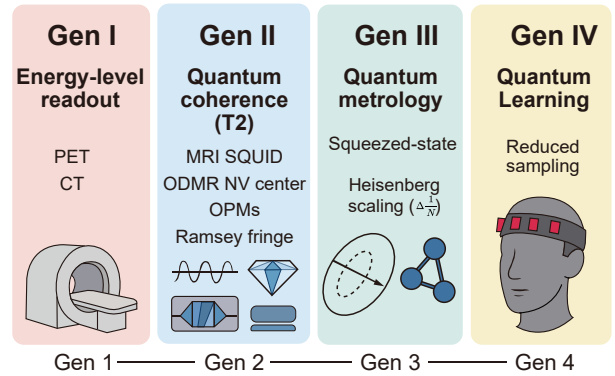


Fig. 1. Conceptual generational map illustrating the technological evolution of quantum biosensing. The diagram delineates three overarching paradigms quantum spectroscopy, quantum metrology, and quantum learning each enabling higher sensitivity and functional integration. The 1st–4th generation biosensors represent successive advances from basic spin readout to coherence-based sensing, entanglement-enhanced metrology, and emerging quantum–AI co-designed medical schemes (Appendix A).

quantum resources they employ. Existing discussions often remain fragmented and platform-specific, making it difficult to identify technological maturity and future development trajectories. Here we propose a generational framework for biomedical quantum sensors that organizes sensing technologies according to the depth of quantum resource utilization. This framework provides conceptual clarity, establishes consistent benchmarks for technological maturity, and identifies the natural progression from physical signal detection toward intelligent quantum-enhanced inference.

Current Landscape of Quantum Biomedical Sensors. Modern biomedical measurement stands at a crossroads between established clinical modalities

* These authors contributed equally to this work.

† Corresponding author: junyuliu@pitt.edu

and emerging technologies that exploit genuine quantum phenomena like coherence and entanglement. Superconducting quantum interference devices (SQUIDs) remain the most mature platform, providing femtoTesla (10^{-15} T) sensitivity essential for detecting neural and cardiac fields in magnetoencephalography (MEG) and magnetocardiography (MCG) [8]. Beyond SQUIDs, coherence-based sensors, such as solid-state NV centers and cold-atom interferometers, have expanded the scope of biometrology to the nanoscale, enabling high-sensitivity, real-time functional readouts [9, 10]. Entanglement-enhanced sensing has further demonstrated precision improvements beyond classical limits in solid-state spin platforms [11, 12]. These developments signal a broader shift: moving from simple physical observations toward hybrid, learning-enabled systems that integrate quantum resources with computational intelligence (Fig. 1).

We delineate four conceptual generations of biomedical quantum sensors, categorized by their utilization of quantum resources and the depth of information integration:

- (I) **Gen I: Energy-Level Readout.** These sensors utilize discrete quantum energy levels as sensing elements but rely on population or spectral readout without maintaining coherent superposition. Operating effectively as classical sensors with quantum-scale transduction, this generation includes MRI, magnetoresistive sensors, and fluorescence spectroscopy [1].
- (II) **Gen II: Quantum Coherence.** This stage exploits quantum coherence such as wave-like spatial or temporal superposition states to measure physical quantities. Achievable precision scales with the coherence time (T_2), a principle demonstrated in solid-state systems like NV centers and atomic interferometers.
- (III) **Gen III: Quantum Metrology.** Third-generation architectures leverage quantum entanglement and spin squeezing to improve sensitivity beyond classical limits. By employing entangled or correlated ensembles, these systems enable information encoding that approaches the Heisenberg limit.
- (IV) **Gen IV: Quantum Learning.** The emerging frontier integrates quantum sensors with quantum or hybrid quantum-classical processors to process measured information adaptively. This paradigm enables data-driven, intelligent sensing and real-time interpretation of biological signals, marking a transition from raw measurement to active learning.

This framework formalizes the evolution of biomedical sensing from observing physical observables to interpreting structured biological information through quantum-enhanced intelligence. The remainder of this Perspective develops the proposed generational framework for biomedical quantum sensing. Section II reviews the foundations of biomedical measurement and

the motivations for quantum sensing. Section III introduces the four sensor generations. Section IV discusses key physical constraints across platforms. The final section outlines future directions toward clinical translation.

II. RELATED WORK

Medical imaging technologies have transformed modern medicine by enabling non-invasive visualization of anatomical, functional, and metabolic processes, beginning with X-rays in 1895 [13], followed by computed tomography (CT) [14] and positron emission tomography (PET) [15]. CT and PET rely strictly on classical radiation detection and are not classified as quantum sensors. Among established clinical technologies, magnetic resonance imaging (MRI) [16, 17] operates on coherent precession of nuclear spins, designating it as a second-generation modality within the generational framework developed here.

Despite their tremendous clinical impact, these imaging modalities rely on fundamentally classical measurement processes whose precision is ultimately constrained by stochastic noise sources. Specifically, thermal noise described by the Johnson–Nyquist theorem [18, 19] sets the minimum detectable signal in resistive systems, while photon shot noise fundamentally limits optical and nuclear imaging [20]. Together with measurement limits such as the SQL [21], these noise sources impose rigid barriers to sensitivity enhancement. These limitations are particularly problematic in applications requiring the detection of extremely weak or highly localized biological signals, including early-stage disease biomarkers [22], single-cell processes [23], and rapid physiological dynamics [24]. Representative examples include neural magnetic fields at the picotesla level, weak molecular signals in early disease stages, and transient physiological processes occurring on millisecond timescales. Beyond sensitivity limitations, classical medical imaging modalities also face important practical constraints, including ionizing radiation exposure in X-ray and CT [25], toxicity risks of gadolinium-based contrast agents required for oncological and vascular MRI [26], limited penetration depth in optical imaging [27], and restricted temporal resolution in metabolic imaging [28]. These challenges have motivated quantum sensing as a promising approach to access elusive physiological signals. Unlike classical energy-based measurements, quantum sensors encode physical parameters into coherent phase evolution of quantum states via quantum superposition [29], while quantum entanglement enables correlated measurements surpassing classical precision bounds [5]. With the quantum Cramér–Rao bound [30] defining ultimate precision limits, these principles establish the foundation for quantum-enhanced biomedical sensing, potentially enabling earlier disease detection, improved functional mapping, and continuous monitoring of physiological processes beyond the reach of existing technologies.

Biomedical environments present one of the most de-

The Multiscale Landscape of Biomedical Quantum Sensing: From Quantum Resources to Clinical Decision Support

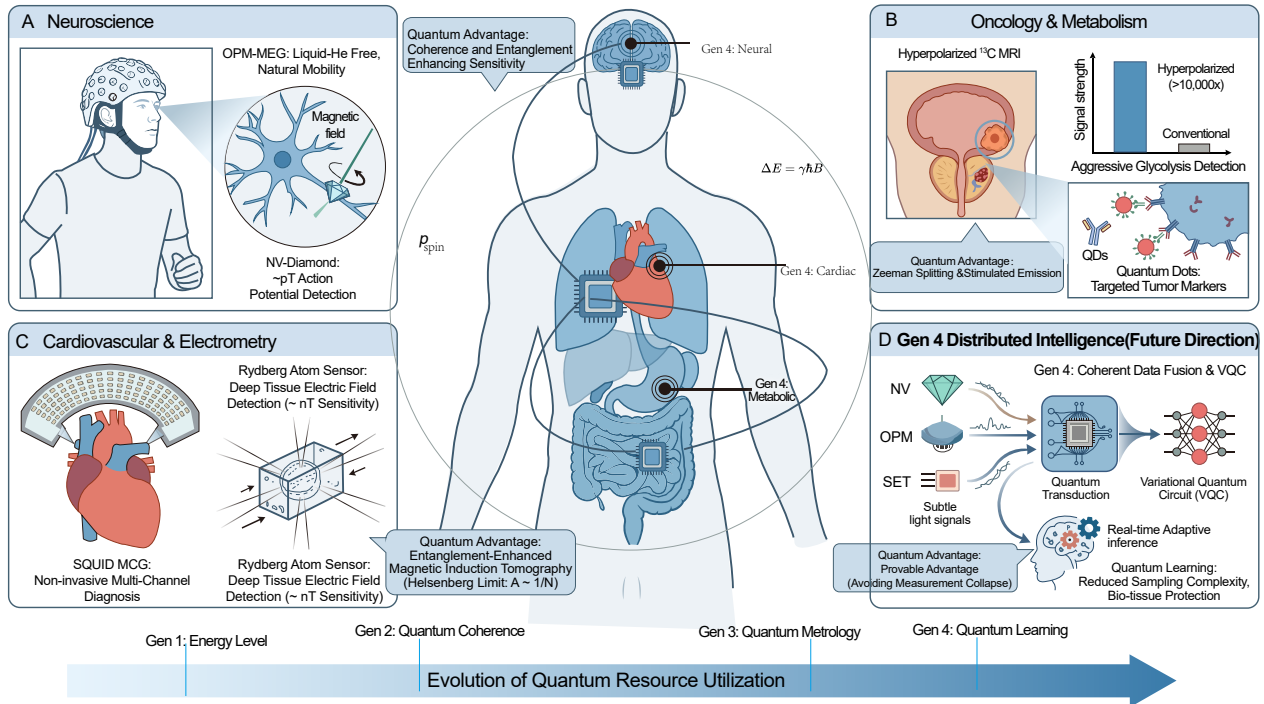


Fig. 2. Multiscale applications and generational evolution of biomedical quantum sensing. **A–C**, Representative clinical deployments across neuroscience, oncology, and cardiovascular medicine, highlighting quantum advantages in Gen 1–3 platforms. **D**, Emerging paradigm of Gen 4 distributed intelligence, featuring coherent data fusion via quantum transduction and adaptive inference through variational quantum circuits (VQC). The bottom axis illustrates the transition from discrete energy-level readout (Gen 1) to advanced quantum learning (Gen 4).

manding operating regimes for quantum sensors, fundamentally mismatched with the isolation and stability typically required for quantum-enhanced measurements. Living biological systems operate in warm, hydrated, and dynamically fluctuating environments that induce rapid decoherence of fragile quantum states [31, 32]. Unlike laboratory quantum sensing platforms that operate under carefully controlled conditions, biomedical sensors must function in open, thermally active, and mechanically unstable environments. As a result, achievable sensitivity, coherence time, and sensing distance are jointly constrained by the physical properties of biological tissue rather than by quantum resources alone [1]. Several dominant noise sources further limit practical performance in clinical settings. Electromagnetic interference from medical instrumentation, power systems, and surrounding electronics introduces broadband background noise, while mechanical motion arising from respiration, cardiac activity, and involuntary patient movement produces time-varying artifacts that degrade signal stability. In addition, magnetic fluctuations from nearby ferromagnetic materials and structural components can distort weak biomagnetic signals [33], imposing stringent requirements on shielding and sensor placement [34]. Beyond environmental noise, translational and clinical constraints impose additional limitations. Many high-performance quantum sensors, such as SQUIDs, rely on cryogenic temperatures and bulky dewar systems [35]. While newer modalities such as optically pumped magnetometers

and NV centers operate at or near room temperature, they still face challenges related to intense optical fields or microwave radiation that may lead to localized tissue heating [36]. Furthermore, biomedical deployment requires strict biocompatibility of sensor packaging [37, 38], non-invasive operation, and adherence to safety guidelines regarding electromagnetic exposure [39]. Consequently, realizing the full potential of biomedical quantum sensing demands the successful integration of intrinsic quantum sensitivity with clinically practical, biologically compatible system designs and workflows.

III. QUANTUM MEDICAL SENSOR GENERATIONS

First Generation Quantum Medical Sensor: Energy-Level Readout.

First-generation quantum sensors rely on quantized energy spectra and spin-dependent interactions of electronic or nuclear states to map biological signals onto measurable energy shifts. In contrast to higher-generation sensors, coherence and superposition are not defining components of the sensing process [1, 3].

Despite relying on relatively simple quantum resources, first-generation quantum sensors have achieved widespread clinical deployment and constitute the backbone of modern medical diagnostics. Representative implementations include magnetoresis-

Table I. Unified comparison of representative first-, second-, and third-generation quantum sensing platforms for biomedical applications. Resolution denotes intrinsic detection capability for 1st/2nd-generation sensors; Gain quantifies the demonstrated improvement beyond the standard quantum limit (SQL) for 3rd-generation platforms. Entanglement resources employed by third-generation sensors are indicated by superscript footnotes (^{a–i}). Biomedical viability is jointly constrained by operating temperature T_{op} , bio-sample thermal compatibility T_{bio} , and sensor–sample distance. T_{bio} reflects the thermal environment experienced by the biological sample, determined jointly by T_{op} and the sensor–sample distance: when the sensor operates in the near field with strong thermal coupling, $T_{\text{bio}} \approx T_{\text{op}}$; when sufficient standoff distance provides thermal isolation, T_{bio} remains at physiological temperature (~ 300 K).

Platform	Gen.	Measured quantity	Resolution / Gain	T_{op}	T_{bio}	Distance
<i>A. First Generation — Energy-Level Readout</i>						
GMR sensors	1st	Magnetoresistance	nT magnetic fields	233–423 K	298–310 K	Near-field
TMR sensors	1st	Tunneling current	nT magnetic fields	233–398 K	298–310 K	< 1 mm
Quantum dots / nanowires	1st	Optical / electrical signal	Molecular sensitivity	~ 300 K	293–318 K	Near-field
SET	1st	Single-electron charge	Single-charge sensitivity	0.01–40 K	0.01–40 K	< 100 nm
NV centers (ensemble)	1st	Local magnetic field	pT–nT magnetic fields	288–333 K	293–310 K	< 1 mm
Muon probes (μSR)	1st	Local magnetic field	High local sensitivity	0.03–1000 K	2–300 K	Near-field
Neutron probes	1st	Magnetic / nuclear contrast	μT –nT contrast	293–303 K	2–300 K	10 cm–1 m
<i>B. Second Generation — Quantum Coherence</i>						
NMR sensors	2nd	Magnetic field	$\propto 1/\sqrt{N}$	~ 4 K	~ 300 K	5 mm–2 cm
MRI / fMRI	2nd	Spin relaxation	$0.47 \text{ fT}/\sqrt{\text{Hz}}$	~ 4 K	~ 300 K	5 mm–2 cm
NV centers (Ramsey/echo)	2nd	Local B-field (ionic)	$< 10 \text{ pT}/\sqrt{\text{Hz}}$	295–300 K	~ 300 K	< 100 nm–1 μm
SQUID	2nd	Magnetic flux	$\text{fT-pT}/\sqrt{\text{Hz}}$	4–20 K	~ 300 K	1–25 mm
OPMs (SERF / Larmor)	2nd	B-field (atomic spin)	$\text{fT-pT}/\sqrt{\text{Hz}}$	393–473 K	~ 300 K	1–5 mm
Rydberg atom sensors	2nd	E-field amplitude	$\text{V cm}^{-1}/\sqrt{\text{Hz}}$	298–353 K	~ 300 K	100–500 μm
Flux qubits [40]	2nd	Magnetic flux var.	$\text{pT}/\sqrt{\text{Hz}}$	≤ 20 mK	≤ 20 mK	~ 1 –10 μm
Charge qubits [41]	2nd	E-field / charge	$10^{-7} e/\sqrt{\text{Hz}}$	≤ 100 mK	≤ 100 mK	< 100 nm
Atom interferometers	2nd	Inertial phase	$10^{-9} g$	μK –100 nK	~ 300 K	< 100 μm
<i>C. Third Generation — Entanglement-Enhanced Metrology</i>						
NV centers (entangled) ^a [11]	3rd	Magnetic field	~ 5 dB	~ 300 K	~ 300 K	< 100 nm
NV ensemble (spin-squeezed) ^b [42]	3rd	Magnetic field	~ 0.5 dB	~ 300 K	~ 300 K	< 1 mm
Optomechanical systems ^c [43]	3rd	Force / displacement	~ 2 dB	4–10 K	4–10 K	Near-field
Trapped ions (entangled) ^d [44]	3rd	Frequency / B-field	4–9 dB	mK regime	~ 300 K	\sim mm
Atomic vapor (spin-squeezed) ^f [45]	3rd	Magnetic field	~ 2 dB	350–470 K	~ 300 K	mm–cm
Atomic vapor (entangled) ^g [46]	3rd	Magnetic gradient	5.5 dB	350–470 K	~ 300 K	cm
Rydberg atom arrays ^h [47]	3rd	Metrological phase	3.5–4 dB	10–100 μK	10–100 μK	Near-field
Optical interferometers ⁱ [48]	3rd	Optical path phase	~ 3 dB	~ 300 K	~ 300 K	mm
Superconducting circuits ^e [49]	3rd	Magnetic flux / force	~ 1 dB	10–20 mK	~ 300 K	< 1 m

^a Bell-state/GHZ (2–3 spins), $\sim \mu\text{s}$ –ms. ^b Dipolar spin squeezing ($\sim 10^3$ spins), $\sim \mu\text{s}$. ^c Squeezed light + mechanical entanglement, steady-state. ^d GHZ/spin squeezing (2–14+ ions), 1 ms–0.1 s. ^e Squeezed microwave vacuum, $\sim \mu\text{s}$. ^f Collective spin squeezing ($\sim 10^{12}$ – 10^{13} atoms), 1–100 ms. ^g Entangled photon–spin correlations, ~ 1 –10 ms. ^h Dipolar spin squeezing (~ 70 –100 atoms), 10–100 μs . ⁱ Photon-pair entanglement (SPDC), ps correlation time.

tive (GMR [50] and TMR [51]), quantum dots [52], NV centers with ODMR readout utilizing the Zeeman effect [38, 53], and incoherent optically pumped magnetometers [54]. Quantum states serve primarily as energy structure enabling signal transduction rather than engineered quantum information carriers, so measurement precision follows classical scaling laws [2] despite the sensing mechanism being of quantum origin [1].

Magnetoresistive biology quantum sensors (Appendix B 1) mainly consist of giant and tunnel magnetoresistance devices (GMR/TMR), which represent early examples of first-generation quantum medical sensing in which spin-dependent electronic transport enables robust signal transduction under ambient conditions. In these platforms, biological events are indirectly encoded through magnetic labels or local fields that modulate electronic resistance. While historically important, such sensors primarily serve as illustrative cases of quantum-enabled transduction rather than as

central drivers of future biomedical quantum sensing.

A complementary class of first-generation quantum sensors operate at the nanoscale through quantization of electronic energy levels and charge. Quantum dots and single-electron (Appendix B 2) devices leverage discrete electronic states, Coulomb blockade, or size-dependent optical emission to detect molecular binding events and biochemical interactions with high sensitivity. These platforms have proven particularly effective in fluorescence-based imaging and label-assisted biosensing, where the stability of quantized states improves signal robustness. However, the quantum states involved function solely as static energy spectra rather than dynamically controlled carriers of information, and measurement precision remains governed by classical statistics.

Nitrogen-vacancy centers in diamond have emerged as a powerful first-generation quantum sensing platform for magnetic imaging at cellular and subcellu-

lar length scales. Although NV-based sensors rely on quantum spin properties of point defects in diamond, first-generation implementations operate through ensemble averaging and optically detected magnetic resonance without exploiting inter-qubit entanglement or actively preserved coherence. Wide-field quantum diamond microscopes employing dense NV ensembles have achieved submicron spatial resolution with sensitivities on the order of two hundred nanotesla, enabling magnetic imaging of individual cells labeled with superparamagnetic nanoparticles [55]. Earlier demonstrations resolved intracellular magnetite chains in living magnetotactic bacteria with approximately four hundred nanometer spatial resolution, establishing NV centers as a viable modality for noninvasive magnetic imaging in biological systems [56]. More recent advances have enabled quantitative immunomagnetic imaging of human tumor sections at micrometer-scale resolution, while remaining compatible with conventional histological and fluorescence workflows [57]. The chemical inertness and biocompatibility of diamond, together with stable room-temperature operation, position NV-based platforms as promising candidates for ex vivo diagnostics and future minimally invasive monitoring applications.

Beyond room-temperature platforms, muon spin spectroscopy (μ SR) and neutron-based probes offer exceptional sensitivity to local magnetic environments and atomic-scale structure, respectively [58, 59]. However, both techniques require large-scale facilities, including particle accelerators for μ SR and nuclear reactors or spallation sources for neutron scattering, that fundamentally preclude point-of-care or in vivo deployment [58, 60]. While neutron capture therapy (BNCT) demonstrates clinical translation potential for cancer treatment [60], these facility-dependent platforms remain confined to ex situ characterization of biological materials, positioning them as complementary research tools rather than candidates for widespread biomedical quantum sensing.

Although the platforms above span diverse implementations, they share a common architectural limitation: quantum states serve only as passive transduction elements, and measurement precision obeys classical scaling ($\Delta\theta \propto 1/\sqrt{N}$) [2]. The performance ceiling is set by classical noise statistics rather than quantum bounds. NV centers make this tension especially visible: the same defect system that supports coherent spin manipulation and entanglement-assisted protocols [38] is, in first-generation implementations, reduced to incoherent ensemble readout. Overcoming this classical precision barrier motivates the transition to second-generation sensors, where quantum coherence is deliberately preserved as a metrological resource.

Second Generation Quantum Medical Sensor: Quantum Coherence.

Second-generation quantum sensors utilize the phase evolution of coherent superpositions to approach the SQL, as demonstrated by phase-sensing interferometers [61], providing a signal-to-noise ratio (SNR) that scales with \sqrt{N} [2, 62]. Table I highlights that only

a small subset of quantum sensors remain biologically viable once thermal and spatial constraints are imposed. Consistent with prior reviews, NMR-based modalities are grouped under second-generation sensors here, though this adopts a broad definition based on quantum coherence; a stricter criterion would distinguish conventional ensemble MRI from coherence-engineered NMR protocols.

Nuclear magnetic resonance (NMR) sensors represent the earliest and most clinically mature class of quantum medical sensors, exploiting coherent precession of thermal nuclear spin ensembles to encode magnetic, chemical, and spatial information. Frequency and phase encoding established MRI as a non-contact modality for anatomical visualization [16], while blood-oxygen-level-dependent (BOLD) contrast enabled functional MRI (fMRI), providing an indirect measure of neural activity through susceptibility-induced modulation of transverse (T_2^*) relaxation [63]. NMR offers deep tissue penetration, physiological-temperature operation, and exceptional chemical specificity, supporting clinical adoption from structural imaging to metabolomics and functional brain mapping [64]. However, spin coherence is rapidly averaged over macroscopic ensembles and is not preserved as an actively controllable metrological resource, constraining sensitivity and temporal resolution to scales dictated by thermal polarization and relaxation rather than quantum coherence. Consequently, MRI performance improvements have relied predominantly on engineering advances in hardware, pulse sequences, and signal processing rather than coherence-enabled scaling. Extensions such as hyperpolarized ^{13}C MRI partially overcome polarization limits for real-time metabolic imaging [65], highlighting both the power and the remaining boundaries of NMR-based quantum sensing.

Second-generation NV diamond magnetometers extend first-generation sensing by preserving spin coherence during measurement, improving sensitivity from the hundred-nanotesla regime to single-digit pT/ $\sqrt{\text{Hz}}$ and enabling label-free detection of intrinsic bioelectric currents. Using a thirteen-micrometer-thick, high-density NV layer, Barry et al. directly measured the ~ 15 pT magnetic pulse from single action potentials in invertebrate axons with ~ 30 μs temporal resolution [9], while biophysical modeling predicts three-dimensional localization of axon-hillock currents with approximately 70% accuracy [66]. Recent advances in pulsed magnetometry have further expanded capability: ensemble NV sensors employing Ramsey or spin-echo sequences with volumes of $\sim 300 \times 100 \times 20$ μm^3 and ~ 50 pT/ $\sqrt{\text{Hz}}$ sensitivity over 10 kHz bandwidth have recorded compound action potentials in live mouse brain slices, with tetrodotoxin perfusion abolishing the signal and confirming its neuronal origin [67]. Material-engineering advances, such as [111]-oriented bulk diamond achieving 9.4 ± 0.1 pT/ $\sqrt{\text{Hz}}$ in continuous-wave mode [68], further improve the baseline sensitivity, although the generational distinction rests on active coherence manipulation rather than on CW readout alone. These results position

NV-diamond magnetometry at the threshold of non-invasive, cellular-scale neurophysiology: unlike electrodes, NV sensors enable contactless recording without tissue damage, and unlike fMRI, which infers neural activity indirectly through hemodynamic responses on second timescales, NV magnetometers directly capture electromagnetic signals with microsecond resolution. Beyond magnetometry, the coherence-based paradigm extends to nanoscale nuclear magnetic resonance: single NV centers combined with dynamic decoupling sequences (e.g., XY8-k) that actively preserve spin coherence have enabled NMR spectroscopy of zeptoliter sample volumes [69], opening routes to label-free monitoring of drug–target binding kinetics and structural characterization of biomolecular complexes under native conditions. This application exemplifies the defining characteristic of second-generation sensing: measurement sensitivity is directly determined by the actively maintained coherence time rather than by ensemble averaging alone. Despite remaining challenges in sensitivity, array scalability, and clinical integration, these coherence-enabled sensors open a path toward transformative applications including intra-operative functional mapping, chronic monitoring of epileptic networks, and high-throughput screening of patient-derived neural organoids.

SQUIDs represent the most clinically mature second-generation quantum sensors, providing unmatched femtotesla-level magnetic field sensitivity through coherence-based phase detection. Although conventional SQUID systems require cryogenic cooling and impose large sensor–source standoff distances, recent on-scalp implementations place sensors in close proximity to biological tissue, substantially improving spatial resolution and signal-to-noise ratio. On-scalp SQUID magnetoencephalography has revealed early somatosensory responses with ~ 16 ms latency that were undetectable using conventional MEG, directly demonstrating the diagnostic value of reduced sensor-to-cortex distance [70]. In cardiology, multi-channel SQUID magnetocardiography has achieved a positive predictive value of approximately 93–95% for inflammatory cardiomyopathy in a cohort of over 200 patients, outperforming conventional echocardiography and enabling superior response tracking [71]. Beyond neural and cardiac applications, SQUID-based magnetoneurography enables noninvasive imaging of spinal and peripheral nerve conduction [72], while ultra-low-field MRI using SQUID detectors demonstrates the feasibility of hybrid MEG/MRI systems operating at microtesla fields [73]. Despite these successes, widespread clinical adoption remains constrained by cryogenic infrastructure, magnetic shielding requirements, and standoff-distance–limited spatial resolution. Ongoing advances in high-temperature superconductors, compact cryocoolers, and signal processing are progressively narrowing the gap between SQUID performance and clinical deployability, positioning SQUIDs as a benchmark platform that motivates the development of room-temperature second-generation alternatives [8].

Second-generation optically pumped magnetometers

(OPMs) exploit coherent precession of spin-polarized alkali vapor ensembles to achieve single-digit femtotesla per root hertz sensitivity at room temperature, eliminating the cryogenic standoff of SQUID-based MEG. On-scalp OPM arrays yield two- to four-fold larger neuronal signal amplitudes while permitting natural head movement. Wearable systems exceeding fifty channels have been deployed clinically in infants and epilepsy patients [74]. An eighty-channel dual-axis OPM helmet has further reproduced visual-evoked and gamma-band responses in twenty healthy adults, including participants whose dental metal precluded conventional MEG recordings, demonstrating robustness under realistic clinical conditions [75]. Beyond neuroimaging, OPM gradiometer arrays enable quantitative magnetorelaxometry of tumor-targeted magnetic nanoparticles: a twenty-two-sensor platform mapped six micrograms of iron across a 12×8 cm² field of view [76], while a pulsed-pump OPM design operating in unshielded environments detected 1.4 micrograms of iron in 100 μ L volumes with bandwidths exceeding 100 kHz [77]. Despite these advances, clinical translation remains limited by manufacturing scalability, thermal management, and magnetic interference rejection in hospital environments. Nevertheless, room-temperature operation, flexible positioning, and scalable architectures position OPMs as strong candidates for next-generation clinical neuroimaging, with emerging applications in portable stroke assessment, bedside monitoring, and multimodal integration with EEG and functional near-infrared spectroscopy.

Rydberg-atom quantum sensors rely critically on vacuum or sealed vapor cells to preserve atomic coherence and enable high-fidelity electrometry. Atoms excited to high principal quantum numbers exhibit extremely large electric dipole moments and polarizabilities, rendering them exquisitely sensitive to external electromagnetic fields but simultaneously highly susceptible to collisional decoherence from background gas molecules. Vacuum or low-pressure vapor cells suppress atom–molecule collisions, stabilize atomic density and temperature, and provide a well-controlled electromagnetic environment required for coherent excitation and optical readout via electromagnetically induced transparency or Autler–Townes splitting [78, 79]. Without such isolation, Rydberg-state lifetimes collapse to nanosecond scales under ambient conditions, eliminating usable coherence and sensing contrast. While these cell-based architectures enable room-temperature operation without cryogenic infrastructure, the requirement for sealed vacuum environments, optical access, and precise field control fundamentally constrains compatibility with *in vivo* biological settings, where close sensor–tissue proximity, mechanical compliance, and environmental robustness are essential. As a result, although Rydberg sensors represent a powerful platform for quantum electrometry, their reliance on vacuum cells remains a primary obstacle to direct biomedical translation [80].

Similar to Rydberg sensors, solid-state qubits and matter-wave interferometers offer extraordinary precision but face severe translational barriers. Flux

qubits are emerging as powerful quantum sensors for biomedical applications, offering sensitivity at the $\text{pT}/\sqrt{\text{Hz}}$ level by transducing small flux changes into shifts of the qubit’s microwave transition [40]. Meanwhile, superconducting charge qubits function as extreme electrometers. A heavy-shunted fluxonium qubit operated at 1.8 MHz recently achieved a charge sensitivity of $33 \mu\text{e}/\sqrt{\text{Hz}}$ [81]. Recent designs of charge qubits (Cooper-pair boxes, CPBs) have achieved $10^{-7} e/\sqrt{\text{Hz}}$ level by coupling a CPB to a microwave resonator and exploiting its quantum nonlinearity [41]. However, these quantum sensors require cryogenic operation and complex microwave control, posing significant challenges to in vivo and clinical use. Cold-atom interferometers exploit matter-wave coherence to achieve exceptional inertial sensing precision, with laboratory gravimeters reaching $10^{-9} g$ sensitivity [82], gyroscopes attaining $3 \times 10^{-10} \text{ rad/s}$ level [83], and fundamental constant measurements achieving fractional precision at the 10^{-11} level. However, their applications are confined to fundamental physics and gravity measurements, with minimal relevance to biomedical sensing due to bulky, cryogenic setups and lack of biological compatibility.

Second-generation quantum medical sensors introduce phase- and coherence-based measurement protocols into biologically compatible sensing platforms. In practice, however, coherence is only partially exploited: most implementations rely on short-lived, weakly controlled coherence within ensembles of effectively independent probes, yielding sensitivities that are ultimately bounded by the SQL. Across NMR, NV centers, SQUIDs, and optically pumped magnetometers, translational progress has therefore been driven primarily by engineering advances such as improved field control, sensor miniaturization, array scaling, and signal processing, rather than by active coherence preservation as a scalable metrological resource. As a result, the practical performance ceiling of second-generation sensors is set by deployability, stability, and system integration rather than by fundamental quantum bounds, leaving substantial metrological headroom that coherence alone cannot access.

Third-Generation Quantum Sensor: Entanglement-Enhanced Metrology.

The third generation of quantum sensing is defined by the deliberate engineering of quantum correlations, including entanglement and spin squeezing, to enhance weak-signal estimation beyond classical limits. Unlike second-generation sensors, which rely on coherent evolution of individual quantum systems, third-generation architectures treat shared many-body correlations as the primary metrological resource, redistributing measurement noise across correlated probes to improve the detectability of weak biological signals without proportionally increasing biological burden. This transition is illustrated schematically in Fig. 3.

This noise redistribution is particularly relevant for biomedical sensing, where signals such as neuronal magnetic fields, spin-labeled biomolecules, and radical-pair dynamics are intrinsically weak, spatially

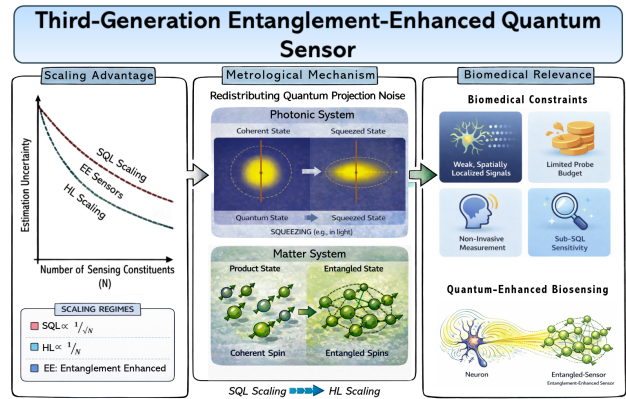


Fig. 3. Entanglement-enhanced biomedical quantum sensing: the 3rd-generation advance.

heterogeneous, and constrained by limits on repetition imposed by biological viability. Improving sensitivity through collective quantum correlations offers enhanced information extraction without increasing measurement backaction or exposure. Among the platforms under active investigation, nitrogen-vacancy centers in diamond and optomechanical systems receive particular attention for their potential room-temperature, biocompatible operation.

The third-generation module in Table I summarizes representative platforms spanning solid-state, atomic, photonic, and superconducting implementations, highlighting the diversity of entanglement resources, measurable quantities, reported sensitivity gains, and sensing distances. While several platforms already operate at or near room temperature, others require cryogenic or ultrahigh-vacuum environments, reflecting differing maturity levels. We briefly discuss representative advances across these platforms.

In nitrogen-vacancy center systems, recent experimental advances have established multiple entanglement-enabled pathways toward improved sensitivity under ambient conditions. Entanglement between an NV electronic spin and a proximal ^{13}C nuclear spin enabled phase estimation beyond uncorrelated limits at room temperature [84]. These concepts were extended to nanoscale sensing by entangling closely spaced NV pairs, leading to enhanced magnetic sensitivity, improved spatial resolution, and common-mode noise rejection when probing external dark spins near the diamond surface [11]. At the multi-qubit level, dipolar interactions have been engineered to generate collective entangled states, including GHZ-like and spin-squeezed states, thereby enhancing the precision of Ramsey-based magnetometry [12]. Related analyses have examined robustness under realistic noise models, showing that moderately entangled states can retain sensitivity gains over uncorrelated probes even in the presence of Markovian decoherence [85]. Schemes exploiting double-quantum transitions, globally addressed microwave control, and qutrit encodings further leverage the full spin-1 Hilbert space of the NV center to accelerate phase accumulation and suppress common-mode noise [86, 87].

Ensemble-scale demonstrations of dipolar-interaction-mediated spin squeezing have additionally shown that correlated many-body states can be generated *in situ* in disordered solids by selectively mitigating strongly coupled spin dimers [42]. Together, these results establish NV centers as a strong solid-state platform for third-generation biomedical sensing, enabling high-sensitivity, minimally invasive interrogation of spin-based biomarkers and dynamic biochemical processes.

Optomechanical platforms provide a distinct third-generation architecture by coupling optical fields to mechanical motion through radiation pressure, enhancing force and displacement sensitivity while reducing technical noise under ambient conditions. Cascaded configurations employing entangled mechanical modes aim to improve force detection and suppress common-mode disturbances [88]. Injection of optical squeezed light into microdisk resonators has enabled magnetometry below the shot-noise limit at room temperature [43]. Direct measurements of quantum backaction correlations have enabled quantum-referenced thermometry without cryogenic cooling [89], while truncated nonlinear interferometry integrated with atomic force microscopy has demonstrated femtometer-scale displacement sensitivity [90]. These advances suggest that optomechanical systems may suit correlation-enhanced sensing of force, displacement, temperature, and magnetic fields in biological environments, though scaling to clinical array formats remains an open challenge.

Trapped-ion systems, while operating under ultrahigh-vacuum conditions, provide a well-established laboratory platform for entanglement-enhanced sensing with long coherence times and high-fidelity quantum control. Early demonstrations established Heisenberg-limited phase scaling using small GHZ states [44], subsequent experiments generated multipartite entangled states of more than ten ions with super-resolved phase evolution [91], and deterministic spin squeezing has produced several decibels of metrological gain [92]. Although not directly deployable, the techniques developed in trapped-ion systems are expected to inform design of more practical platforms.

At the macroscopic scale, atomic vapor systems, particularly those operating in the spin-exchange relaxation-free regime, represent room-temperature platforms for entanglement-enhanced magnetometry with direct relevance to clinical neuroimaging and cardiology. Quantum non-demolition measurements in dense alkali vapors have produced singlet-type correlations among more than 10^{13} atoms, generating measurable spin squeezing and spatially extended entanglement [93]. Complementary approaches based on stroboscopic back-action-evading measurements have prepared spin-squeezed states in cesium vapor magnetometers, achieving several decibels of squeezing and improving magnetic induction tomography sensitivity beyond classical limits [45]. Entanglement-assisted magnetic induction tomography has further demonstrated substantial noise reduction and improved spa-

tial resolution, highlighting the potential of vapor-based systems for imaging weakly conductive biological tissue [45]. Gradiometric configurations employing entangled twin beams have enabled simultaneous suppression of ambient magnetic interference and photon shot noise, achieving femtotesla-scale gradient sensitivity in unshielded environments [46]. Beyond these experimental demonstrations, theoretical proposals suggest that engineered collective dynamics, including quantum-chaotic driving, may further enhance sensitivity in vapor-phase magnetometers without requiring entangled initial states [94]. For clinical applications such as magnetoencephalography, fetal cardiology, and noninvasive conductivity imaging, vapor-based systems are plausible near-term candidates.

Cold-atom Rydberg systems provide another atomic architecture for third-generation quantum sensing, leveraging large electric dipole moments and tunable long-range interactions. Initial demonstrations using these ensembles have achieved microwave electrometry approaching the standard quantum limit, achieving nanovolt-per-centimeter sensitivities over megahertz bandwidths [95]. Although these initial demonstrations relied primarily on coherent control rather than engineered entanglement, subsequent experiments have realized two-atom entanglement near nanophotonic surfaces, enabling micrometer-scale electric field gradient sensing within decoherence-free subspaces [96]. Complementary theoretical proposals based on Rydberg dressing predict the generation of spin-squeezed states in extended two-dimensional atomic arrays through engineered long-range interactions [97]. Rydberg interaction arrays have also demonstrated several-decibel spin squeezing in two-dimensional geometries, underscoring the metrological potential of engineered long-range interactions [47]. Such array-based architectures naturally support spatially multiplexed sensing and suggest a scalable route toward distributed quantum sensor networks capable of imaging weak electric and magnetic field gradients in biological tissues.

Photonic interferometer architectures exploit engineered optical correlations, including squeezing, twin-beam intensity correlations, and entangled photon pairs, to redistribute measurement noise across correlated modes, improving information extraction per photon while remaining compatible with biologically constrained illumination. Quantum-enhanced Raman microscopy and nonlinear interferometric imaging have demonstrated sub-shot-noise sensitivity for chemical contrast and live-cell imaging [98, 99]. Interferometric phase-imaging with entangled photons has achieved scan-free wide-field sensitivity improvements for protein microarray detection [100], while entangled-photon interferometry has enabled adaptive aberration correction in scattering media [101]. Quantum optical coherence tomography leverages Hong–Ou–Mandel interference for dispersion cancellation and enhanced axial resolution in multilayer biological samples, with recent phase-dependent protocols suppressing cross-reflection artifacts [48, 102]. These photonic approaches enhance sensitivity and imaging fidelity with-

out increasing illumination intensity, a critical constraint where photodamage must be minimized.

In contrast to room-temperature solid-state and optical approaches, superconducting architectures, including qubits, resonators, and parametric amplifiers, provide a cryogenic implementation of third-generation quantum sensing. Their strong nonlinearities and precise quantum control enable the preparation and manipulation of nonclassical states, including squeezing and multipartite entanglement, for enhanced measurement precision. Experiments have demonstrated criticality-enhanced force sensing by operating Josephson parametric oscillators near bifurcation points, achieving near-quantum-limited detection of sub-attoNewton forces with potential relevance for ultrasensitive mechanical biosensing [103]. In parallel, graph-state-based quantum magnetometry has been proposed as a noise-resilient entanglement strategy for magnetic field detection [104]. In the microwave domain, squeezed vacuum fields generated by parametric amplifiers have enhanced sensitivity in magnetic resonance spectroscopy, enabling improved detection of weak spin ensembles relevant to biochemical and materials systems [49]. Quantum illumination protocols using entangled microwave-optical photon pairs have further demonstrated sensitivity advantages for detecting low-reflectivity targets in thermal environments, suggesting potential pathways toward noninvasive biomedical imaging [105]. Additionally, optimization-based control techniques applied to tunable superconducting qubits have enabled accelerated and adaptive sensing protocols, with potential applicability to dynamic signal tracking in complex environments [106]. These developments illustrate how cryogenic superconducting platforms can leverage engineered quantum correlations for high-precision sensing, while also highlighting the practical trade-offs associated with low-temperature operation in biomedical contexts.

Third-generation quantum sensors demonstrate that engineered quantum correlations can now be prepared and characterized across a range of platforms operating under increasingly practical conditions, including room-temperature and ambient environments. Entanglement-enhanced sensitivity has been demonstrated in controlled laboratory settings, but the extent to which these scaling advantages persist in biologically complex systems remains uncertain and depends on decoherence, geometry, and integration constraints. Current implementations therefore represent a significant advance in correlation engineering rather than a completed route to clinical performance gains. In many platforms, entangled probe preparation, adaptive control, and hardware-level optimization are already embedded in the sensing protocol itself. This convergence of state engineering and protocol design points toward a fourth generation in which sensing, processing, and inference would operate within a single quantum architecture, bypassing the classical readout stage that currently separates measurement from analysis.

Fourth Generation Quantum Medical Sensor:

Quantum Learning.

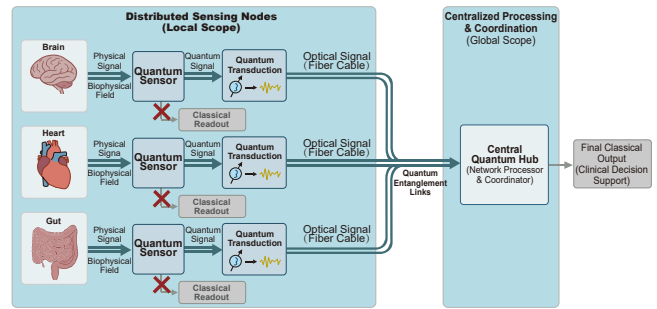


Fig. 4. System architecture of the **fourth-generation quantum medical sensor**. Quantum signals originating from biological targets are captured by quantum sensors (e.g., NV centers), transmitted via optical quantum transduction, and processed either locally or within a coordinated sensor network. The quantum processor performs quantum learning or inference tasks before producing classical outputs for downstream medical analysis. The dashed components indicate optional centralized coordination, which is disabled in fully distributed sensor-network operation where each node performs independent quantum processing and participates in entanglement-based sensing protocols.

Fourth-generation quantum medical sensors represent a qualitative departure from earlier biomedical sensing architectures by eliminating the classical measurement bottleneck. Earlier quantum sensors ultimately collapse quantum states into classical readouts at an intermediate stage, discarding quantum correlations before downstream processing. In contrast, fourth-generation systems are defined by the end-to-end integration of quantum sensing with quantum computation and quantum learning: sensors forward quantum states directly to downstream quantum processors, enabling coherent processing without intermediate classical readout, and supporting distributed sensing networks [107, 108]. In the remainder of this section, we first examine the quantum learning advantages that underpin this generation, then describe the network architectures that enable multi-node sensing, and finally discuss the role of quantum transduction in bridging heterogeneous platforms and enabling coherent quantum information transfer across nodes.

Quantum learning advantage. Fourth-generation quantum medical sensors derive a central part of their advantage from the integration of quantum learning directly into the sensing pipeline, enabling information to be extracted with reduced sample complexity and enhanced precision. This capability is particularly critical in biomedical contexts, where repeated probing may disrupt biological function, cause tissue damage, or expose patients to harmful stimulation. Recent theoretical and experimental work has established provable quantum advantages in learning from experiments, demonstrating reductions in both the number of required quantum state copies and the total experimental time [109–112].

A prominent application of these advantages is

learning the dynamics of unknown systems, typically parameterized as $H(\theta) = \sum_j \theta_j H_j$. By leveraging coherent phase accumulation and entanglement-assisted measurements, quantum protocols can achieve Heisenberg-limited scaling, requiring only $\mathcal{O}(\varepsilon^{-1})$ total evolution time to reach precision ε , strictly outperforming the $\mathcal{O}(\varepsilon^{-2})$ scaling inherent to classical strategies [110]. Furthermore, under suitable access models, quantum methods exponentially reduce the number of distinct experiments required, scaling only polylogarithmically with the target precision [109, 110]. These theoretical gains in sampling efficiency are clinically meaningful in biomedical settings, where minimizing excessive probing is critical to avoiding tissue disruption or harmful radiation exposure. The classical shadow framework further enables efficient simultaneous prediction of many observables from a small number of quantum state copies [110, 113]. Instead of fully reconstructing the sensor-generated quantum state, the protocol applies random unitaries followed by computational-basis measurements to produce classical shadows from which a large family of observables can be estimated. For a set $\mathcal{F} = \{O_j\}$ of sensing-relevant observables, the number of state copies required to estimate all $y_j(u) = \text{Tr}(O_j \rho(u))$ within additive error ε with high probability scales as

$$N_{\text{copies}} = \mathcal{O}\left(\frac{\max_j \text{Var}[\hat{y}_j] \cdot \log |\mathcal{F}|}{\varepsilon^2}\right), \quad (1)$$

yielding a logarithmic dependence on the number of target observables $|\mathcal{F}|$, in contrast to the linear scaling of independent estimation or the exponential cost of full state tomography. This logarithmic scaling might in principle enable multimodal biomedical monitoring, where a single measurement campaign simultaneously characterizes multiple field components, spectral features, or spatial modes under tight acquisition-time constraints. A further fundamental advantage arises from quantum memory: learners that can coherently store and jointly process multiple state copies before choosing which measurements to perform are provably more efficient than classical learners restricted to measurement transcripts. For certain observable families, this separation is exponential in the number of required experimental interactions [110].

Quantum-enhanced hypothesis testing leverages entangled states and coherent measurements to discriminate between candidate physical models or detect weak signals with fewer experimental resources than any classical strategy permits [111, 112]. When quantum sensors are connected to processors capable of joint entangling operations, the resulting measurement statistics might resolve binary or multi-class hypotheses, such as the presence of a biomarker or the classification of tissue pathology, with error probabilities that decrease exponentially faster per sample than classical bounds allow. Crucially, these learning-theoretic improvements are not mutually exclusive with traditional metrological gains but can be compounded within a single sensing protocol, potentially enabling diagnostic workflows that are simultaneously more precise, less invasive, and more informative than existing classical or coherence-only approaches.

The theoretical advantages described above, including Heisenberg-limited Hamiltonian learning, exponential separations in shadow tomography, and quantum-enhanced hypothesis testing, rely on coherent multi-copy processing or entanglement-assisted measurements that presuppose fault-tolerant quantum hardware beyond current capabilities. As a complementary near-term strategy, variational quantum circuits (VQCs) pursue a fundamentally different form of quantum learning: rather than implementing provably optimal protocols, VQCs use parameterized circuits optimized via hybrid quantum-classical loops to maximize task-specific objectives such as the quantum Fisher information [114–116]. Although this heuristic approach sacrifices provable optimality for hardware compatibility, early demonstrations on NV center ensembles and superconducting platforms suggest that meaningful sensing enhancements are achievable within current noise and connectivity constraints. Complementary approaches, such as the incorporation of quantum logic operations and assisted quantum memory in solid-state platforms, have further demonstrated suppression of readout noise, addressing one of the primary bottlenecks in spin-based biomedical sensing.

Despite these advances, practical deployment faces significant latency challenges. VQCs require iterative hybrid optimization loops in which a classical co-processor repeatedly updates circuit parameters based on measurement outcomes, with end-to-end latency per optimization step reaching milliseconds to seconds depending on circuit depth, parameter count, and shot budget. For biomedical applications demanding real-time feedback, such as intraoperative neural monitoring or closed-loop neurostimulation, these timescales may exceed clinically relevant thresholds. Whether near-term quantum processors can satisfy such timing constraints while maintaining sufficient circuit expressibility and noise resilience remains an open translational challenge.

Quantum sensor networks. A quantum sensor network jointly operates multiple quantum sensors while preserving quantum resources across nodes. Only networks that maintain quantum coherence or entanglement qualify as genuine quantum sensor networks; those that merely aggregate classical readouts cannot sustain quantum advantage after measurement-induced collapse. These networks divide into two regimes: local and distributed, each addressing different biomedical constraints. Local quantum sensor networks consist of co-located homogeneous sensors (e.g., NV center ensembles or arrays within a single organ) that can be entangled locally for enhanced sensitivity and noise suppression through collective quantum effects. Because all nodes operate on the same physical carrier and are spatially proximate, quantum states are generated, manipulated, and consumed entirely within a single platform, enabling entanglement-assisted sensing without inter-platform conversion or quantum transduction. This regime is well suited for array-level biomedical measurements where multiple probes must jointly monitor a spatially extended target while remaining physically accessible for local entan-

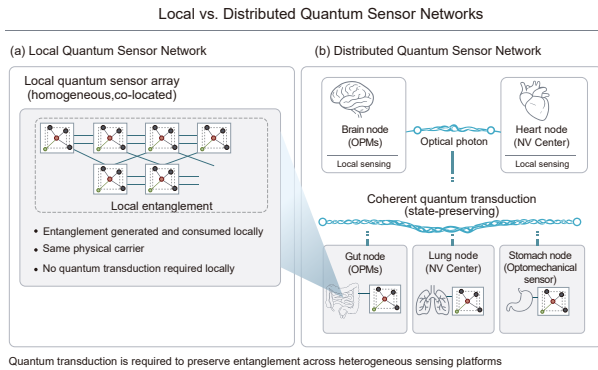


Fig. 5. Conceptual comparison between a **local quantum sensor network** and a **distributed quantum sensor network**. In the local configuration, entanglement is generated and consumed entirely within a co-located sensor array, eliminating the need for quantum transduction. In contrast, the distributed sensor network connects spatially separated sensing nodes (e.g., brain, cardiac, or gastric sensors) via quantum transduction, enabling long-range quantum correlations across heterogeneous biological sites.

gling operations.

Distributed quantum sensor networks arise when sensors are spatially separated or physically heterogeneous, as occurs when probes span distinct organs or clinical sites. Different sensor types (e.g., NV centers, optomechanical transducers) encode quantum information in incompatible physical carriers, forcing current protocols to measure at each node individually and aggregate classical data. This intermediate readout irreversibly destroys coherence, entanglement, and high-dimensional Hilbert-space correlations [117, 118], projecting the exponentially rich state of an n -qubit system into a low-dimensional classical record. The premature-measurement problem is therefore the central bottleneck separating classical sensor fusion from genuine quantum-enhanced distributed sensing.

Quantum transduction. Quantum transduction addresses the premature-measurement bottleneck identified above by coherently converting quantum states between heterogeneous physical carriers without intermediate classical readout [119, 120]. Unlike classical transducers that convert analog signals between physical domains, quantum transduction must preserve the full quantum state including superposition and entanglement, imposing stringent constraints on conversion fidelity, added noise, and bandwidth. By converting quantum states, rather than classical signals, into a common carrier (typically optical photons at telecom wavelengths for long-distance transmission), transduction ensures that sensor-generated quantum resources remain available for joint processing across nodes [119, 120]. The resulting distributed architecture supports *joint inference*: simultaneous extraction of correlated information from anatomically separated sensors that is inaccessible through independent classical measurements. Entanglement-enhanced precision enables distributed protocols to surpass the standard quantum limit and approach Heisenberg-limited scaling [107, 121, 122], while a network of M entan-

gled nodes with n qubits each operates in a 2^{Mn} -dimensional joint Hilbert space, providing exponential representational advantage over classical fusion of M independent records [123]. Quantum transduction is therefore not merely a peripheral engineering challenge but a necessary architectural component that delineates the boundary between third- and fourth-generation quantum medical sensing systems.

The progression from current demonstrations to fully distributed quantum medical sensor networks will proceed through several intermediate stages. In the *near term* (approximately 2025–2030), the most accessible implementations are local entangled sensor arrays, such as NV center ensembles or co-located OPM clusters, that exploit intra-platform entanglement for enhanced sensitivity without requiring quantum transduction or long-range coherence. In the *mid term* (approximately 2030–2040), advances in transduction fidelity and quantum memory lifetimes are expected to enable point-to-point quantum links between a small number of heterogeneous sensor nodes within a single clinical suite [119]. In the *long term* (beyond 2040), contingent on fault-tolerant quantum computation and scalable quantum networking, distributed quantum data centers could provide the computational backbone for population-scale medical sensing, hosting quantum processors, quantum random-access memory (QRAM) with $\mathcal{O}(\log N)$ -time access to quantum data entries [124, 125], and network interfaces that enable coherent aggregation of sensor data from geographically distributed clinical facilities.

IV. CROSS-CUTTING CONSIDERATIONS

Bandwidth Matching and Neural Signal Hierarchy

The generational classification introduced above describes biomedical quantum sensors according to the depth of quantum resources employed, ranging from energy-level readout in first-generation devices to entanglement-enhanced metrology and quantum learning in later generations. However, the suitability of a sensing platform for a specific biomedical application depends not only on quantum resource depth but also on several orthogonal physical parameters. Bandwidth is defined as the frequency range over which a sensor maintains useful sensitivity, emerges as a fundamental and often underappreciated dimension. Unlike sensitivity, which can often be improved through engineering strategies such as averaging or array scaling, bandwidth is fundamentally constrained by the underlying sensing mechanism. As a result, bandwidth and generational classification form two independent axes: sensors of the same quantum generation may exhibit very different usable bandwidths depending on their physical implementation.

From a neurophysiological perspective, the fastest canonical electrical signal produced by neurons is the action potential, with a characteristic duration of approximately 1 ms (1 kHz), a limit set by ion-channel refractory dynamics rather than engineering constraints.

Table II. Bandwidth matching between neural signal hierarchy and quantum sensing platforms. The header row shows each platform’s usable bandwidth; suitability is indicated as: \checkmark (well matched), \circ (marginal), \times (mismatched).

Signal Type	Frequency	SQUID	OPM	NV Center
<i>Sensor bandwidth</i>		DC– \sim 1 kHz [126, 127]	\sim 100–200 Hz [33, 128, 129]	DC–kHz–GHz [130–132]
Cortical rhythms (α, β, γ) [133]	<100 Hz	\checkmark	\checkmark	\checkmark
High-gamma oscillations	80–200 Hz	\checkmark	\circ	\checkmark
Evoked responses (MEG/MCG)	1–100 Hz	\checkmark	\checkmark	\checkmark
Peripheral nerve CAPs [134]	100 Hz–5 kHz	\circ	\times	\checkmark
Single-neuron action potentials	\sim 1 kHz	\times	\times	\checkmark
Fast invasive LFP	1–8 kHz	\times	\times	\checkmark
Ion-channel gating dynamics	10–100 kHz	\times	\times	\circ
Molecular processes (MHz) [135]	>1 MHz	\times	\times	\checkmark [69]

Overqualified: NV bandwidth exceeds signal requirements; sensitivity may be the limiting factor.

Resolving individual neuronal spikes or microcircuit-level dynamics therefore requires sensing modalities capable of operating in the kilohertz regime and in close spatial proximity to the signal source. Experimentally recorded brain signals represent the superposition of many asynchronously firing neurons, producing a broad spectral distribution; recent invasive recordings have reported local field potential activity extending into the 2–8 kHz range in pathological conditions such as epilepsy [136]. At even smaller spatial scales, ion-channel gating dynamics occur on timescales from tens of μ s to milliseconds, corresponding to frequencies from hundreds of hertz to tens of kilohertz [137].

The temporal hierarchy of neural and physiological signals and the corresponding bandwidth requirements are summarized in Table II, together with the characteristic bandwidths of representative quantum sensing platforms.

OPMs, particularly those operating in the SERF regime, achieve femtotesla-level sensitivity but typically exhibit bandwidths limited to approximately DC–200 Hz [33, 128]. This bandwidth is well matched to conventional MEG, whose signal content lies primarily below a few hundred hertz [127], but fundamentally restricts access to faster neural dynamics such as spike-level or microcircuit activity. Moreover, current OPM systems are designed for macroscopic, far-field measurements with sensor–source distances on the order of centimeters, inherently averaging over large neural populations and suppressing spatially localized or high-frequency components.

In contrast, solid-state NV centers in diamond inherently support broadband magnetic sensing owing to their fast spin dynamics and room-temperature operation [130, 132]. In near-field geometries, where sensor–source distances can be reduced to the micrometer-to-millimeter scale, magnetic fields scale as $1/r^3$, enabling NV sensors to access fast, localized neural signals in the kHz regime and beyond. However, near-field operation currently limits NV magnetometry to surface-accessible or surgically exposed tissue, and single-sensor sensitivity in the picotesla regime remains insufficient for detecting deep cortical sources at macroscopic standoff distances.

Bridging Clinical Bottlenecks and Technological Maturity

The successful clinical translation of quantum sensing hinges on a strategic alignment between the depth of quantum resource utilization and the multifaceted demands of biological environments. As systematically mapped in Table III, established diagnostic modalities have largely reached performance ceilings dictated by classical physics and infrastructure limitations. Conventional MRI, for instance, is constrained by exceptionally low thermal spin polarization ($\sim 10^{-5}$), necessitating prolonged acquisition times and absolute patient immobility. Similarly, the reliance of SQUID-based MEG on cryogenic cooling (~ 4 K) imposes rigid dewar geometries that force a significant sensor-to-source standoff distance, inherently suppressing weak biomagnetic signals. A more granular breakdown of these specific device bottlenecks and their physical origins is provided in Table V (Appendix C).

Quantum sensors address these unmet clinical needs by leveraging coherence and entanglement to redefine the boundaries of sensitivity and accessibility. Second-generation platforms, such as OPMs, represent a pivotal breakthrough by eliminating cryogenic requirements and enabling wearable, high-density arrays. This transition addresses the primary bottleneck of “immobility” in neuroimaging, offering a three- to fivefold signal gain through reduced standoff distance while permitting natural subject movement. For metabolic oncology, the integration of hyperpolarized ^{13}C overcomes polarization limits to provide $> 10,000\times$ signal enhancement [65], enabling real-time, radiation-free metabolic imaging where traditional PET remains limited by cyclotron dependence and ionizing exposure. The historical evolution of these sensitivity gains across different sensing modalities is summarized in Table VI (Appendix C).

Within the multiscale landscape of biomedical sensing, NV centers in diamond are particularly suited to near-field, high-bandwidth applications requiring resolution of localized microcircuits. Crucially, these two modalities are not competitors but clinical complements: OPMs excel at whole-brain network monitoring and wearable neuroimaging, while NV sensors are uniquely positioned for near-field, high-bandwidth

Table III. Clinical needs versus quantum sensor capability matching across representative biomedical applications. Each row identifies a specific unmet clinical need, the core limitations of existing devices, the most suitable quantum sensing platform (with generational classification), the physical origin of the quantum advantage, and the key translational bottleneck. TRL (Technology Readiness Level) values follow the NASA/Mankins scale and refer specifically to the developmental stage of the Best-Matched Quantum Platform in the context of the identified clinical need, ranging from basic principles (TRL 1) to system flight proven through mission operations (TRL 9) [138].

Clinical Domain	Unmet Clinical Need	Limitations of Existing Devices	Requirement Parameters	Best-Matched Quantum Platform (Gen.)	Origin of Quantum Advantage	TRL	Key Translational Bottleneck
A. Neuroscience							
Whole-brain functional imaging	ms-resolved whole-brain imaging during natural movement	fMRI: BOLD delay ~ 5 s, immobility; SQUID-MEG: rigid helmet, ~ 200 units globally; EEG: localization error up to 25 mm	< 50 ft/ $\sqrt{\text{Hz}}$; < 1 ms; non-ionizing	OPM-MEG (2nd Gen.) wearable array	Cryogen-free wearable \rightarrow 3-5 \times signal gain; 15-sensor OPM \approx 62-ch SQUID	5-7	MSR still required; sensor scalability; insufficient clinical validation
Single-neuron electrophysiology	Non-invasive single-neuron AP detection	Microelectrodes: invasive; fMRI: ~ 1 Hz; MEG/EEG: cannot resolve single cells	~ 10 pT; ~ 30 μ s; < 100 μ m; near-field	NV-diamond magnetometer (2nd Gen.)	μ m standoff $\rightarrow 1/r^3$ gain $\rightarrow \sim 15$ pT single AP; NV Center kHz-GHz bandwidth	3-5	532 nm penetration 6.5%/mm; surface only; sensitivity gap 1-2 orders
Pre-surgical epilepsy localization	High-precision seizure-focus mapping replacing iEEG	iEEG: craniotomy, high risk; SQUID-MEG: inaccessible; EEG: poor localization	< 20 ft/ $\sqrt{\text{Hz}}$; < 5 ms; non-invasive	OPM-MEG (2nd Gen.) high-density array	On-scalp \rightarrow higher sampling; ictal recording feasible; He-4 OPM validated	6-7	510(k) pathway clear; large-scale trials needed; EMI management
Early neurodegenerative detection	Pre-symptomatic biomarkers for AD/PD	MRI: structural lag; PET-A β : radiation, costly; EEG: insufficient sensitivity	Subtle rhythm changes; ms-scale; safe for repeated monitoring	OPM-MEG (2nd) + quantum learning (4th Gen.)	α/β rhythm detection; wearable \rightarrow longitudinal; Gen 4: adaptive inference	4-6	Biomarker validation lacking; cohort studies needed; data standardization
B. Oncology							
Early cancer metabolic detection	Detect metabolic abnormalities before morphological changes	PET-FDG: 4-5 mm, low Stage I lung; CT/MRI: phenotypic	Single-cell metabolism; < 1 mm; no radiation; repeatable	Hyperpol. ^{13}C MRI (1st \rightarrow 2nd Gen.)	$> 10,000\times$ enhancement \rightarrow real-time metabolic imaging; Warburg; no radiation	5-6	Short $T_1 \sim 60$ s; requires DNP; cost and workflow
Molecular tumor imaging	Specific labeling and micro-metastasis visualization	Gd: non-specific, nephrotoxic; PET: cytotron; fluorescence: photobleaching, shallow	Molecular sensitivity; target-specific; low toxicity; > 1 cm penetration	Quantum dots (1st Gen.) NIR fluorescence	Size-tunable NIR \rightarrow deep penetration; peptide \rightarrow targeting	4-6	Cd-QD toxicity; non-degradable; De Novo regulatory
Intraop. margin assessment	Real-time tumor boundary ID during surgery	Intraop MRI: slow; frozen section: 20-30 min; fluorescence: limited specificity	< 100 μ m; real-time; non-destructive; surgery-compatible	NV wide-field magnetic imaging (1st-2nd Gen.)	Immunomagnetic labeling \rightarrow NV wide-field; sub-cellular resolution	3-4	Surface only; pre-labeling; workflow not validated
C. Cardiology							
Inflammatory cardiomyopathy screening	Non-invasive rapid screening	Echo: operator-dependent; MRI: slow, expensive; ECG: insensitive to deep lesions	\sim pT; real-time; multi-channel; non-invasive	SQUID-MCG (2nd Gen.) \rightarrow OPM-MCG	SQUID-MCG: PPV 93-95%; OPM: cryogen-free \rightarrow portable; contactless	SQUID 7-8; OPM 5-6	SQUID: cost; OPM-MCG: validation needed; no reimbursement
Fetal cardiac monitoring	Non-invasive fetal arrhythmia diagnosis	Fetal ECG: maternal contamination; fetal echo: poor temporal resolution	\sim pT; through maternal tissue; absolute safety; ms-scale	OPM array (2nd Gen.) unshielded gradiometer	B -field unattenuated through tissue; undistorted fetal signal; wearable	5-6	Maternal motion artifacts; interference; protocol standardization
D. Molecular / Cellular Detection							
Intracellular label-free sensing	Real-time $T/pH/B$ inside living cells	Fluorescent probes: photobleaching; EM: fixed samples; optical: diffraction ~ 200 nm	< 100 nm; non-toxic; quantitative	Fluorescent nanodiamond (1st-2nd Gen.)	Chemically inert; nanoscale thermometry (\sim mK); single-protein NMR	4-5	Size control; sub-toxic stress; research-to-IVD path
Single-molecule biomarker detection	Ultra-sensitive detection at ultra-low concentrations	ELISA: LOD \sim pM; mass spec: sample prep; PCR: nucleic acids only	Single-molecule; specific; rapid (POC); affordable	SET/QD (1st Gen.) + NV relaxometry (2nd Gen.)	SET: single-charge; NV: wash-free immunoassay; QD-FRET: molecular distance	3-5	SET: cryogenics; NV standardization; competing digital ELISA
E. Distributed Multi-Organ Monitoring (Future)							
Multi-organ coordinated monitoring	Simultaneous brain-heart-gut quantum-correlated monitoring	Current multimodal: classical fusion only; no cross-organ quantum correlations	Distributed; entanglement preserved; adaptive real-time inference	Distributed QSN (4th Gen.)	Quantum transduction across heterogeneous nodes; VQC optimization; Heisenberg $\Delta \sim 1/N$	1-3	Transduction efficiency low; biological decoherence; > 10 yr

interrogation of fast neural dynamics at the single-neuron and microcircuit level, as detailed in the bandwidth hierarchy of Table III.

V. CONCLUSION

In this perspective, we introduced a generational framework that organizes the evolution of biomedical quantum sensors according to the depth of quantum resources employed, spanning energy-level readout in first-generation systems, coherence-based metrology in second-generation platforms, engineered entanglement and squeezing in third-generation architectures, and integrated quantum learning and information-processing strategies in a prospective fourth generation. This taxonomy provides conceptual clarity in a rapidly expanding field where technological maturity, physical constraints, and quantum resource utilization are often treated interchangeably.

First-generation platforms demonstrate that the presence of quantized energy levels alone does not guarantee quantum advantage. Second-generation sensors harness coherent phase evolution as a metrological resource and have achieved clinically meaningful deployment in technologies such as MRI, SQUID-based magnetometry, and optically pumped magnetometers, although many implementations remain limited by partial coherence utilization and ensemble averaging rather than fundamental quantum scaling. Third-generation architectures introduce a qualitative transition by deliberately engineering many-body correlations to redistribute measurement noise and enhance sensitivity; experimental demonstrations across solid-state, atomic, photonic, and superconducting systems confirm measurable gains under controlled laboratory conditions, even as translation to complex biological environments remains constrained by decoherence, scalability, and integration challenges. The proposed fourth generation extends this trajectory by embedding sensing within broader quantum information-processing architectures. By integrating adaptive control, variational optimization, distributed networks, and transduction interfaces, these systems aim to enable data-driven inference directly at the physical layer, particularly in biomedical contexts where safety and invasiveness limit measurement repetition. However, quantum processing and learning impose substantial computational demands: variational quantum circuits require iterative classical-quantum optimization loops whose cost scales with circuit depth, qubit count, and the number of variational parameters, while distributed quantum sensor networks add communication and synchronization overhead. Whether these computational requirements can be met within the real-time latency constraints of clinical decision-making, such as intraoperative guidance or continuous physiological monitoring, remains an open and important deployment challenge.

Beyond clinical translation, quantum sensors are opening new avenues in fundamental medical science that merit equal emphasis. At the subcellular scale,

nitrogen-vacancy magnetometry has enabled direct observation of magnetic signatures from individual neurons, magnetotactic bacteria, and immunolabeled tumor sections, providing experimental access to biological phenomena that were previously below the detection threshold of any existing technique. In pharmacology and drug discovery, quantum computing and nanoscale quantum sensors are enabling molecular simulation of protein-drug interactions and label-free, real-time monitoring of drug-target binding kinetics at the single-molecule level, complementing conventional high-throughput screening with mechanistic insight [139, 140]. Nanoscale nuclear magnetic resonance enabled by single NV centers has achieved chemical spectroscopy of zeptoliter sample volumes, establishing a new experimental paradigm for structural biology of membrane proteins, metabolites, and biomolecular complexes under native conditions. These contributions to basic biomedical research, spanning biophysics, neuroscience, oncology, and pharmacology, demonstrate that the impact of quantum sensing extends well beyond clinical diagnostics and should inform the prioritization of future research directions alongside clinical integration efforts.

Generational depth alone does not determine biomedical suitability. Bandwidth, sensor-sample geometry, thermal compatibility, and clinical safety impose independent constraints that shape practical deployment, and physiological processes span spatial and temporal regimes that no single platform fully addresses. Near-term milestones, such as demonstrating entanglement-enhanced sensitivity in a biological sample under ambient conditions or conducting initial clinical validation of third-generation protocols, will be important for testing whether laboratory-scale quantum gains translate into measurable diagnostic improvements. Continued progress will require coordinated advances in quantum resource engineering, device physics, and biologically informed system design, alongside careful experimental validation. The transition from energy-level readout to entanglement-enabled and learning-integrated architectures therefore reflects not only increasing quantum complexity but an expanding ambition: to move from measuring isolated observables toward extracting structured biological information under realistic clinical constraints.

Acknowledgements.—JL is supported in part by the University of Pittsburgh, School of Computing and Information, Department of Computer Science, Pitt Cyber, PQI Community Collaboration Awards, John C. Mascaró Faculty Scholar in Sustainability, NASA under award number 80NSSC25M7057, and Fluor Marine Propulsion LLC (U.S. Naval Nuclear Laboratory) under award number 140449-R08. G.D. and J.B. are supported by National Science Foundation Award No. 2304998. KPS thanks the U.S. Department of Energy, Office of Science, Advanced Scientific Computing Research (ASCR) program, for support under Award Number DE-SC0026264, and PQI Community Collaboration Awards.

-
- [1] C. L. Degen, F. Reinhard, and P. Cappellaro, *Quantum sensing*, *Rev. Mod. Phys.* **89**, 035002 (2017).
- [2] V. Giovannetti, S. Lloyd, and L. Maccone, *Quantum-enhanced measurements: beating the standard quantum limit*, *Science* **306**, 1330 (2004).
- [3] N. Aslam, H. Zhou, E. K. Urbach, M. J. Turner, R. L. Walsworth, M. D. Lukin, and H. Park, *Quantum sensors for biomedical applications*, *Nature Reviews Physics* **5**, 157 (2023).
- [4] S. Bakhshandeh, *Quantum sensing goes bio*, *Nature Reviews Materials* **7**, 254 (2022).
- [5] V. Giovannetti, S. Lloyd, and L. Maccone, *Advances in quantum metrology*, *Nature Photonics* **5**, 222 (2011).
- [6] T. Zhang, G. Pramanik, K. Zhang, M. Gulka, L. Wang, J. Jing, F. Xu, Z. Li, Q. Wei, P. Cigler, et al., *Toward quantitative bio-sensing with nitrogen-vacancy center in diamond*, *ACS sensors* **6**, 2077 (2021).
- [7] M. Zwierz, C. A. Pérez-Delgado, and P. Kok, *Ultimate limits to quantum metrology and the meaning of the heisenberg limit*, *Physical Review A—Atomic, Molecular, and Optical Physics* **85**, 042112 (2012).
- [8] R. Fenici, M. Picerni, P. Fenici, and D. Brisinda, *An advanced vision of magnetocardiography as an unrivalled method for a more comprehensive non-invasive clinical electrophysiological assessment*, *American Heart Journal Plus: Cardiology Research and Practice* **52**, 100514 (2025).
- [9] J. F. Barry, M. J. Turner, J. M. Schloss, D. R. Glenn, Y. Song, M. D. Lukin, H. Park, and R. L. Walsworth, *Optical magnetic detection of single-neuron action potentials using quantum defects in diamond*, *Proceedings of the National Academy of Sciences* **113**, 14133 (2016).
- [10] J. Taylor, P. Cappellaro, L. Childress, L. Jiang, D. Budker, P. Hemmer, A. Yacoby, R. Walsworth, and M. Lukin, *High-sensitivity diamond magnetometer with nanoscale resolution*, *Nature Physics* **4**, 810 (2008).
- [11] X. Zhou, M. Wang, X. Ye, H. Sun, Y. Guo, S. Han, Z. Chai, W. Ji, K. Xia, F. Shi, Y. Wang, and J. Du, *Entanglement-enhanced nanoscale single-spin sensing*, *Nature* **647**, 883 (2025).
- [12] J. Rovny, S. Kolkowitz, and N. P. de Leon, *Multi-qubit nanoscale sensing with entanglement as a resource*, *Nature* **647**, 876 (2025).
- [13] W. C. Röntgen, *Über eine neue art von strahlen*, *Sitzungsberichte der Physikalisch-Medicinischen Gesellschaft zu Würzburg* , 132 (1895).
- [14] G. N. Hounsfield, *Computerized transverse axial scanning (tomography): Part 1. description of system*, *The British journal of radiology* **46**, 1016 (1973).
- [15] M. M. Ter-Pogossian, M. E. Phelps, E. J. Hoffman, and N. A. Mullani, *A positron-emission transaxial tomograph for nuclear imaging (pett)*, *Radiology* **114**, 89 (1975).
- [16] P. C. Lauterbur, *Image formation by induced local interactions: examples employing nuclear magnetic resonance*, *nature* **242**, 190 (1973).
- [17] P. Mansfield, *Multi-planar image formation using nmr spin echoes*, *Journal of Physics C: Solid State Physics* **10**, L55 (1977).
- [18] J. B. Johnson, *Thermal agitation of electricity in conductors*, *Physical review* **32**, 97 (1928).
- [19] H. Nyquist, *Thermal agitation of electric charge in conductors*, *Physical review* **32**, 110 (1928).
- [20] L. Mandel and E. Wolf, *Optical coherence and quantum optics* (Cambridge university press, 1995).
- [21] C. M. Caves, *Quantum-mechanical noise in an interferometer*, *Physical Review D* **23**, 1693 (1981).
- [22] S. M. Hanash, S. J. Pitteri, and V. M. Faca, *Mining the plasma proteome for cancer biomarkers*, *Nature* **452**, 571 (2008).
- [23] S. J. Altschuler and L. F. Wu, *Cellular heterogeneity: do differences make a difference?*, *Cell* **141**, 559 (2010).
- [24] C. Orphanidou, *A review of big data applications of physiological signal data*, *Biophysical reviews* **11**, 83 (2019).
- [25] D. J. Brenner and E. J. Hall, *Computed tomography—an increasing source of radiation exposure*, *New England journal of medicine* **357**, 2277 (2007).
- [26] P. Caravan, J. J. Ellison, T. J. McMurry, and R. B. Lauffer, *Gadolinium (iii) chelates as mri contrast agents: structure, dynamics, and applications*, *Chemical reviews* **99**, 2293 (1999).
- [27] V. Ntziachristos, *Going deeper than microscopy: the optical imaging frontier in biology*, *Nature methods* **7**, 603 (2010).
- [28] J. A. Sorenson, M. E. Phelps, et al., *Physics in nuclear medicine* (Grune & Stratton New York, 1987).
- [29] V. Giovannetti, S. Lloyd, and L. Maccone, *Quantum metrology*, *Physical Review Letters* **96**, 010401 (2006).
- [30] C. W. Helstrom, *Minimum mean-squared error of estimates in quantum statistics*, *Physics Letters A* **25**, 101 (1967).
- [31] M. Schlosshauer, *Decoherence and the quantum-to-classical transition* (Springer, 2007).
- [32] M. A. Taylor and W. P. Bowen, *Quantum metrology and its application in biology*, *Physics Reports* **615**, 1 (2016).
- [33] E. Boto, N. Holmes, J. Leggett, G. Roberts, V. Shah, S. S. Meyer, L. D. Muñoz, K. J. Mullinger, T. M. Tierney, S. Bestmann, et al., *Moving magnetoencephalography towards real-world applications with a wearable system*, *Nature* **555**, 657 (2018).
- [34] T. M. Tierney, N. Holmes, S. Mellor, J. D. López, G. Roberts, R. M. Hill, E. Boto, J. Leggett, V. Shah, M. J. Brookes, et al., *Optically pumped magnetometers: From quantum origins to multi-channel magnetoencephalography*, *NeuroImage* **199**, 598 (2019).
- [35] M. Hämmäläinen, R. Hari, R. J. Ilmoniemi, J. Knuu-tila, and O. V. Lounasmaa, *Magnetoencephalography—theory, instrumentation, and applications to noninvasive studies of the working human brain*, *Reviews of modern Physics* **65**, 413 (1993).
- [36] Y. Wu, F. Jelezko, M. B. Plenio, and T. Weil, *Diamond quantum devices in biology*, *Angewandte Chemie International Edition* **55**, 6586 (2016).
- [37] B. D. Ratner, A. S. Hoffman, F. J. Schoen, and J. E. Lemons, *Biomaterials science: an introduction to materials in medicine*, *San Diego, California* **5**, 162 (2004).
- [38] R. Schirhagl, K. Chang, M. Loretz, and C. L. Degen, *Nitrogen-vacancy centers in diamond: nanoscale sensors for physics and biology*, *Annual Review of Physical Chemistry* **65**, 83 (2014).
- [39] I. C. on Non-Ionizing Radiation Protection et al., *Guidelines for limiting exposure to electromagnetic fields (100 khz to 300 ghz)*, *Health physics* **118**, 483

- (2020).
- [40] H. Toida, K. Sakai, T. F. Teshima, M. Hori, K. Kakuyanagi, I. Mahboob, Y. Ono, and S. Saito, *Magnetometry of neurons using a superconducting qubit*, *Communications Physics* **6**, 19 (2023).
- [41] J. Tanarom and P. Gomasang, in *2024 International Conference on Photonics Solutions (ICPS2024)*, Vol. 13518 (SPIE, 2025) pp. 54–59.
- [42] W. Wu, E. J. Davis, L. B. Hughes, B. Ye, Z. Wang, D. Kufel, T. Ono, S. A. Meynell, M. Block, C. Liu, H. Yang, A. C. Bleszynski Jayich, and N. Y. Yao, *Spin squeezing in an ensemble of nitrogen–vacancy centres in diamond*, *Nature* **646**, 74 (2025).
- [43] B.-B. Li, J. Bílek, U. B. Hoff, L. S. Madsen, S. Forstner, V. Prakash, C. Schäfermeier, T. Gehring, W. P. Bowen, and U. L. Andersen, *Quantum enhanced optomechanical magnetometry*, *Optica* **5**, 850 (2018).
- [44] D. Leibfried, M. D. Barrett, T. Schaetz, J. Britton, J. Chiaverini, W. M. Itano, J. D. Jost, C. Langer, and D. J. Wineland, *Toward heisenberg-limited spectroscopy with multiparticle entangled states*, *Science* **304**, 1476 (2004).
- [45] W. Zheng, H. Wang, R. Schmieg, A. Oesterle, and E. S. Polzik, *Entanglement-enhanced magnetic induction tomography*, *Phys. Rev. Lett.* **130**, 203602 (2023).
- [46] S. Wu, G. Bao, J. Guo, J. Chen, W. Du, M. Shi, P. Yang, L. Chen, and W. Zhang, *Quantum magnetic gradiometer with entangled twin light beams*, *Science Advances* **9**, eadg1760 (2023).
- [47] G. Bornet, G. Emperauger, C. Chen, B. Ye, M. Block, M. Bintz, J. A. Boyd, D. Barredo, T. Comparin, F. Mezzacapo, T. Roscilde, T. Lahaye, N. Y. Yao, and A. Browaeys, *Scalable spin squeezing in a dipolar rydberg atom array*, *Nature* **621**, 728 (2023).
- [48] M. Y. Li-Gomez, T. Hrushevskiy, K. McArthur, P. Yepiz-Graciano, A. B. U'Ren, and S. Barzanjeh, *Phase-dependent quantum optical coherence tomography*, *Physical Review Research* **7**, 043039 (2025).
- [49] A. Bienfait, P. Campagne-Ibarcq, A. H. Küllerich, X. Zhou, S. Probst, J. J. Pla, T. Schenkel, D. Vion, D. Esteve, J. J. L. Morton, K. Moelmer, and P. Bertet, *Magnetic resonance with squeezed microwaves*, *Phys. Rev. X* **7**, 041011 (2017).
- [50] D. R. Baselt, G. U. Lee, M. Natesan, S. W. Metzger, P. E. Sheehan, and R. J. Colton, *A biosensor based on magnetoresistance technology*, *Biosensors and Bioelectronics* **13**, 731 (1998).
- [51] C. Ghemes, O.-G. Dragos-Pinzaru, M. Tibu, M. Lostun, N. Lupu, and H. Chiriac, *Tunnel magnetoresistance-based sensor for biomedical application: proof-of-concept*, *Coatings* **13**, 227 (2023).
- [52] X. Michalet, F. F. Pinaud, L. A. Bentolila, J. M. Tsay, S. Doose, J. J. Li, G. Sundaresan, A. Wu, S. Gambhir, and S. Weiss, *Quantum dots for live cells, in vivo imaging, and diagnostics*, *science* **307**, 538 (2005).
- [53] L. Rondin, J.-P. Tetienne, T. Hingant, J.-F. Roch, P. Maletinsky, and V. Jacques, *Magnetometry with nitrogen-vacancy defects in diamond*, *Reports on Progress in Physics* **77**, 056503 (2014).
- [54] B. Zhao, L. Li, Y. Zhang, J. Tang, Y. Liu, and Y. Zhai, *Optically pumped magnetometers recent advances and applications in biomagnetism: A review*, *IEEE Sensors Journal* **23**, 18949 (2023).
- [55] D. R. Glenn, K. Lee, H. Park, R. Weissleder, A. Yacoby, M. D. Lukin, H. Lee, R. L. Walsworth, and C. B. Connolly, *Single-cell magnetic imaging using a quantum diamond microscope*, *Nature methods* **12**, 736 (2015).
- [56] D. Le Sage, K. Arai, D. R. Glenn, S. J. DeVience, L. M. Pham, L. Rahn-Lee, M. D. Lukin, A. Yacoby, A. Komeili, and R. L. Walsworth, *Optical magnetic imaging of living cells*, *Nature* **496**, 486 (2013).
- [57] S. Chen, W. Li, X. Zheng, P. Yu, P. Wang, Z. Sun, Y. Xu, D. Jiao, X. Ye, M. Cai, *et al.*, *Immuno-magnetic microscopy of tumor tissues using quantum sensors in diamond*, *Proceedings of the National Academy of Sciences* **119**, e2118876119 (2022).
- [58] A. D. Hillier, S. J. Blundell, I. McKenzie, I. Umegaki, L. Shu, J. A. Wright, T. Prokscha, F. Bert, K. Shimomura, A. Berlie, *et al.*, *Muon spin spectroscopy*, *Nature Reviews Methods Primers* **2**, 4 (2022).
- [59] H. Rauch and S. A. Werner, *Neutron Interferometry: Lessons in Experimental Quantum Mechanics, Wave-Particle Duality, and Entanglement*, Vol. 12 (Oxford University Press, 2015).
- [60] T. D. Malouff, D. S. Seneviratne, D. K. Ebner, W. C. Stross, M. R. Waddle, D. M. Trifiletti, and S. Krishnan, *Boron neutron capture therapy: a review of clinical applications*, *Frontiers in oncology* **11**, 601820 (2021).
- [61] R. S. Bondurant and J. H. Shapiro, *Squeezed states in phase-sensing interferometers*, *Physical Review D* **30**, 2548 (1984).
- [62] C. M. Caves, *Quantum-mechanical noise in an interferometer*, *Phys. Rev. D* **23**, 1693 (1981).
- [63] S. Ogawa, D. W. Tank, R. Menon, J. M. Ellermann, S. G. Kim, H. Merkle, and K. Ugurbil, *Intrinsic signal changes accompanying sensory stimulation: functional brain mapping with magnetic resonance imaging.*, *Proceedings of the National Academy of Sciences* **89**, 5951 (1992).
- [64] T. Buerge, J. Steinfeldt, G. Ruyoga, M. Pietzner, D. Bizzarri, D. Vojinovic, J. U. z. Belzen, L. Look, P. Kittner, L. Christmann, N. Hollmann, H. Strangalies, J. M. Braunger, B. Wild, S. T. Chiesa, *et al.*, *Metabolomic profiles predict individual multidisease outcomes*, *Nature Medicine* **28**, 2309 (2022).
- [65] N. Sushentsev, M. A. McLean, A. Y. Warren, A. J. Benjamin, C. Brodie, A. Frary, A. B. Gill, J. Jones, J. D. Kaggie, B. W. Lamb, *et al.*, *Hyperpolarised ^{13}C -mri identifies the emergence of a glycolytic cell population within intermediate-risk human prostate cancer*, *Nature Communications* **13**, 466 (2022).
- [66] M. Parashar, K. Saha, and S. Bandyopadhyay, *Axon hillock currents enable single-neuron-resolved 3d reconstruction using diamond nitrogen-vacancy magnetometry*, *Communications physics* **3**, 174 (2020).
- [67] N. W. Hansen, J. L. Webb, L. Troise, C. Olsson, L. Tomasevic, O. Brinza, J. Achard, R. Staacke, M. Kieschnick, J. Meijer, *et al.*, *Microscopic-scale magnetic recording of brain neuronal electrical activity using a diamond quantum sensor*, *Scientific reports* **13**, 12407 (2023).
- [68] N. Sekiguchi, M. Fushimi, A. Yoshimura, C. Shinei, M. Miyakawa, T. Taniguchi, T. Teraji, H. Abe, S. Onoda, T. Ohshima, *et al.*, *Diamond quantum magnetometer with dc sensitivity of sub-10 pt hz- $1/2$ toward measurement of biomagnetic field*, *Physical Review Applied* **21**, 064010 (2024).
- [69] I. Lovchinsky, A. Sushkov, E. Urbach, N. P. de Leon, S. Choi, K. De Greve, R. Evans, R. Gertner, E. Bersin, C. Müller, *et al.*, *Nuclear magnetic resonance detection and spectroscopy of single proteins using quantum logic*, *Science* **351**, 836 (2016).

- [70] J. Iivanainen, R. Zetter, M. Grön, K. Hakkarainen, and L. Parkkonen, *On-scalp meg system utilizing an actively shielded array of optically-pumped magnetometers*, *NeuroImage* **194**, 244 (2019).
- [71] D. Brala, T. Thevathasan, S. Grahl, S. Barrow, M. Violano, H. Bergs, A. Golpour, P. Suwalski, W. Poller, C. Skurk, *et al.*, *Application of magneto-cardiography to screen for inflammatory cardiomyopathy and monitor treatment response*, *Journal of the American Heart Association* **12**, e027619 (2023).
- [72] Y. Adachi and S. Kawabata, *Squid magnetoneurography: an old-fashioned yet new tool for noninvasive functional imaging of spinal cords and peripheral nerves*, *Frontiers in Medical Technology* **6**, 1351905 (2024).
- [73] Q. Guo, C. Ma, X. Zhang, Y. Xu, M. Fan, P. Yu, T. Hu, Y. Chang, and X. Yang, *Squid-based magnetic resonance imaging at ultra-low field using the backprojection method*, *Concepts in Magnetic Resonance Part B* **2020**, 8882329 (2020).
- [74] M. J. Brookes, J. Leggett, M. Rea, R. M. Hill, N. Holmes, E. Boto, and R. Bowtell, *Magnetoencephalography with optically pumped magnetometers (opm-meg): the next generation of functional neuroimaging*, *Trends in Neurosciences* **45**, 621 (2022).
- [75] K. Safar, M. M. Vandewouw, J. Sato, J. Devasagayam, R. M. Hill, M. Rea, M. J. Brookes, and M. J. Taylor, *Using optically pumped magnetometers to replicate task-related responses in next generation magnetoencephalography*, *Scientific Reports* **14**, 6513 (2024).
- [76] A. Jaufenthaler, P. Schier, T. Middelman, M. Liebl, F. Wiekhorst, and D. Baumgarten, *Quantitative 2d magnetorelaxometry imaging of magnetic nanoparticles using optically pumped magnetometers*, *Sensors* **20**, 753 (2020).
- [77] A. Jaufenthaler, T. Kornack, V. Lebedev, M. E. Limes, R. Körber, M. Liebl, and D. Baumgarten, *Pulsed optically pumped magnetometers: Addressing dead time and bandwidth for the unshielded magnetorelaxometry of magnetic nanoparticles*, *Sensors* **21**, 1212 (2021).
- [78] J. A. Sedlacek, A. Schwettmann, H. Kübler, R. Löw, T. Pfau, and J. P. Shaffer, *Microwave electrometry with rydberg atoms in a vapour cell using bright atomic resonances*, *Nature physics* **8**, 819 (2012).
- [79] C. L. Holloway, J. A. Gordon, S. Jefferts, A. Schwarzkopf, D. A. Anderson, S. A. Miller, N. Thaicharoen, and G. Raithel, *Broadband rydberg atom-based electric-field probe for si-traceable, self-calibrated measurements*, *IEEE Transactions on Antennas and Propagation* **62**, 6169 (2014).
- [80] H. Fan, S. Kumar, J. Sedlacek, H. Kübler, S. Karimkashi, and J. P. Shaffer, *Atom based rf electric field sensing*, *Journal of Physics B: Atomic, Molecular and Optical Physics* **48**, 202001 (2015).
- [81] B.-L. Najera-Santos, R. Rousseau, K. Gerashchenko, H. Patange, A. Riva, M. Villiers, T. Briant, P.-F. Cohadon, A. Heidmann, J. Palomo, *et al.*, *High-sensitivity ac-charge detection with a mhz-frequency fluxonium qubit*, *Physical Review X* **14**, 011007 (2024).
- [82] V. Ménoret, P. Vermeulen, N. Le Moigne, S. Bonvalot, P. Bouyer, A. Landragin, and B. Desruelle, *Gravity measurements below 10⁻⁹ g with a transportable absolute quantum gravimeter*, *Scientific reports* **8**, 12300 (2018).
- [83] D. Savoie, M. Altorio, B. Fang, L. Sidorenkov, R. Geiger, and A. Landragin, *Interleaved atom interferometry for high-sensitivity inertial measurements*, *Science advances* **4**, eaau7948 (2018).
- [84] G.-Q. Liu, Y.-R. Zhang, Y.-C. Chang, J.-D. Yue, H. Fan, and X.-Y. Pan, *Demonstration of entanglement-enhanced phase estimation in solid*, *Nature Communications* **6**, 6726 (2015).
- [85] T. Sichanugrist, H. Fukuda, T. Moroi, K. Nakayama, S. Chigusa, N. Mizuochi, M. Hazumi, and Y. Matsuzaki, *Entanglement-enhanced ac magnetometry in the presence of markovian noise*, *Phys. Rev. A* **111**, 042605 (2025).
- [86] M. Morillas-Rozas, A. López-García, and J. Cerrillo, *Entanglement generation on the double quantum transition of nv ground state via globally addressing microwave pulse*, arXiv preprint arXiv:2501.18244 10.48550/arXiv.2501.18244 (2025).
- [87] L. Gassab and O. E. Mustecaplıoglu, *Spin squeezing enhanced quantum magnetometry with nitrogen-vacancy center qutrits*, *New Journal of Physics* **27**, 084502 (2025).
- [88] Y. Xia, A. R. Agrawal, C. M. Pluchar, A. J. Brady, Z. Liu, Q. Zhuang, D. J. Wilson, and Z. Zhang, *Entanglement-enhanced optomechanical sensing*, *Nature Photonics* **17**, 470 (2023).
- [89] T. P. Purdy, K. E. Grutter, K. Srinivasan, and J. M. Taylor, *Quantum correlations from a room-temperature optomechanical cavity*, *Science* **356**, 1265 (2017).
- [90] R. C. Pooser, N. Savino, E. Batson, J. L. Beckey, J. Garcia, and B. J. Lawrie, *Truncated nonlinear interferometry for quantum-enhanced atomic force microscopy*, *Phys. Rev. Lett.* **124**, 230504 (2020).
- [91] T. Monz, P. Schindler, J. T. Barreiro, M. Chwalla, D. Nigg, W. A. Coish, M. Harlander, W. Hänsel, M. Hennrich, and R. Blatt, *14-qubit entanglement: Creation and coherence*, *Phys. Rev. Lett.* **106**, 130506 (2011).
- [92] J. G. Bohnet, B. C. Sawyer, J. W. Britton, M. L. Wall, A. M. Rey, M. Foss-Feig, and J. J. Bollinger, *Quantum spin dynamics and entanglement generation with hundreds of trapped ions*, *Science* **352**, 1297 (2016).
- [93] J. Kong, R. Jiménez-Martínez, C. Troullinou, V. G. Lucivero, G. Tóth, and M. W. Mitchell, *Measurement-induced, spatially-extended entanglement in a hot, strongly-interacting atomic system*, *Nature Communications* **11**, 2415 (2020).
- [94] L. J. Fiderer and D. Braun, *Quantum metrology with quantum-chaotic sensors*, *Nature Communications* **9**, 1351 (2018).
- [95] H.-T. Tu, K.-Y. Liao, H.-L. Wang, Y.-F. Zhu, S.-Y. Qiu, H. Jiang, W. Huang, W. Bian, H. Yan, and S.-L. Zhu, *Approaching the standard quantum limit of a rydberg-atom microwave electrometer*, *Science Advances* **10**, eads0683 (2024).
- [96] P. L. Ocola, I. Dimitrova, B. Grinkemeyer, E. Guardado-Sanchez, T. Đorđević, P. Samutpraphoot, V. Vuletić, and M. D. Lukin, *Control and entanglement of individual rydberg atoms near a nanoscale device*, *Phys. Rev. Lett.* **132**, 113601 (2024).
- [97] J. A. Hines, S. V. Rajagopal, G. L. Moreau, M. D. Wahrman, N. A. Lewis, O. Marković, and M. Schleier-Smith, *Spin squeezing by rydberg dressing in an array of atomic ensembles*, *Phys. Rev. Lett.* **131**, 063401 (2023).
- [98] C. A. Casacio, L. S. Madsen, A. Terrasson,

- M. Waleed, K. Barnscheidt, B. Hage, M. A. Taylor, and W. P. Bowen, *Quantum-enhanced nonlinear microscopy*, *Nature* **594**, 201 (2021).
- [99] A. Terrasson, N. P. Mauranyapin, C. A. Casacio, J. Q. Grim, K. Barnscheidt, B. Hage, M. A. Taylor, and W. P. Bowen, *Fast biological imaging with quantum-enhanced raman microscopy*, *Opt. Express* **32**, 36193 (2024).
- [100] R. Camphausen, Álvaro Cuevas, L. Duempelmann, R. A. Terborg, E. Wajs, S. Tisa, A. Ruggeri, I. Cusini, F. Steinlechner, and V. Pruneri, *A quantum-enhanced wide-field phase imager*, *Science Advances* **7**, eabj2155 (2021), <https://www.science.org/doi/pdf/10.1126/sciadv.abj2155>
- [101] P. Cameron, B. Courme, C. Vernière, R. Pandya, D. Faccio, and H. Defienne, *Adaptive optical imaging with entangled photons*, *Science* **383**, 1142 (2024), <https://www.science.org/doi/pdf/10.1126/science.adk7825>.
- [102] P. Yepiz-Graciano, Z. Ibarra-Borja, R. Ramírez Alarcón, G. Gutiérrez-Torres, H. Cruz-Ramírez, D. Lopez-Mago, and A. B. U'Ren, *Quantum optical coherence microscopy for bioimaging applications*, *Phys. Rev. Appl.* **18**, 034060 (2022).
- [103] G. Beaulieu, F. Minganti, S. Frasca, M. Scigliuzzo, S. Felicetti, R. Di Candia, and P. Scarlino, *Criticality-Enhanced Quantum Sensing with a Parametric Superconducting Resonator*, *PRX Quantum* **6**, 020301 (2025), arXiv:2409.19968 [quant-ph].
- [104] P. T. Nguyen, T. K. Le, H. Q. Nguyen, and L. B. Ho, *Harnessing graph state resources for robust quantum magnetometry under noise*, *Scientific Reports* **14**, 20528 (2024).
- [105] S. Barzanjeh, S. Pirandola, D. Vitali, and J. M. Fink, *Microwave quantum illumination using a digital receiver*, *Science Advances* **6**, eabb0451 (2020).
- [106] S. Danilin, N. Nugent, and M. Weides, *Quantum sensing with tunable superconducting qubits: optimization and speed-up*, *New Journal of Physics* **26**, 103029 (2024).
- [107] Z. Zhang and Q. Zhuang, *Distributed quantum sensing*, *Quantum Science and Technology* **6**, 043001 (2021).
- [108] S.-R. Zhao, Y.-Z. Zhang, W.-Z. Liu, J.-Y. Guan, W. Zhang, C.-L. Li, B. Bai, M.-H. Li, Y. Liu, L. You, et al., *Field demonstration of distributed quantum sensing without post-selection*, *Physical Review X* **11**, 031009 (2021).
- [109] H.-Y. Huang, Y. Tong, D. Fang, and Y. Su, *Learning many-body hamiltonians with heisenberg-limited scaling*, *Physical Review Letters* **130**, 200403 (2023).
- [110] H.-Y. Huang, M. Broughton, J. Cotler, S. Chen, J. Li, M. Mohseni, H. Neven, R. Babbush, R. Kueng, J. Preskill, et al., *Quantum advantage in learning from experiments*, *Science* **376**, 1182 (2022).
- [111] C. Oh, S. Chen, Y. Wong, S. Zhou, H.-Y. Huang, J. A. Nielsen, Z.-H. Liu, J. S. Neergaard-Nielsen, U. L. Andersen, L. Jiang, et al., *Entanglement-enabled advantage for learning a bosonic random displacement channel*, *Physical Review Letters* **133**, 230604 (2024).
- [112] Z.-H. Liu, R. Brunel, E. E. Østergaard, O. Cordero, S. Chen, Y. Wong, J. A. Nielsen, A. B. Bregnsbo, S. Zhou, H.-Y. Huang, et al., *Quantum learning advantage on a scalable photonic platform*, *Science* **389**, 1332 (2025).
- [113] H.-Y. Huang, R. Kueng, and J. Preskill, *Predicting many properties of a quantum system from very few measurements*, *Nature Physics* **16**, 1050 (2020).
- [114] N. Arunkumar, K. S. Olsson, J. T. Oon, C. A. Hart, D. B. Bucher, D. R. Glenn, M. D. Lukin, H. Park, D. Ham, and R. L. Walsworth, *Quantum logic enhanced sensing in solid-state spin ensembles*, *Physical Review Letters* **131**, 100801 (2023).
- [115] Q. Zhuang and Z. Zhang, *Physical-layer supervised learning assisted by an entangled sensor network*, *Physical Review X* **9**, 041023 (2019).
- [116] P. Srivastava, V. Kumar, G. Dutt, and K. P. Seshadreesan, *Variational quantum sensing for structured linear function estimation*, arXiv preprint arXiv:2507.22043 10.1109/qce65121.2025.10455 (2025).
- [117] A. S. Holevo, *Bounds for the quantity of information transmitted by a quantum communication channel*, *Problemy Peredachi Informatsii* **9**, 3 (1973).
- [118] S. Aaronson, *The complexity of quantum states and transformations: from quantum money to black holes*, arXiv preprint arXiv:1607.05256 10.48550/arXiv.1612.05903 (2016).
- [119] C. Zhong, X. Han, and L. Jiang, *Quantum transduction with microwave and optical entanglement*, arXiv preprint arXiv:2202.04601 10.1364/quantum.2022.qth4a.2 (2022).
- [120] N. Lauk, N. Sinclair, S. Barzanjeh, J. P. Covey, M. Saffman, M. Spiropulu, and C. Simon, *Perspectives on quantum transduction*, *Quantum Science and Technology* **5**, 020501 (2020).
- [121] W. Ge, K. Jacobs, Z. Eldredge, A. V. Gorshkov, and M. Foss-Feig, *Distributed quantum metrology with linear networks and separable inputs*, *Physical Review Letters* **121**, 043604 (2018).
- [122] Z. Eldredge, M. Foss-Feig, J. A. Gross, S. L. Rolston, and A. V. Gorshkov, *Optimal and secure measurement protocols for quantum sensor networks*, *Physical Review A* **97**, 042337 (2018).
- [123] S. Lloyd, *Quantum machine learning for data classification*, *Physics* **14**, 79 (2021).
- [124] J. Liu, C. T. Hann, and L. Jiang, *Data centers with quantum random access memory and quantum networks*, *Physical Review A* **108**, 032610 (2023).
- [125] J. Liu and L. Jiang, *Quantum data center: Perspectives*, *IEEE Network* **38**, 160 (2024).
- [126] J. Clarke and A. I. Braginski, *The SQUID handbook: fundamentals and technology of SQUIDS and SQUID systems* (John Wiley & Sons, 2006).
- [127] S. Baillet, *Magnetoencephalography for brain electrophysiology and imaging*, *Nature neuroscience* **20**, 327 (2017).
- [128] V. K. Shah and R. T. Wakai, *A compact, high performance atomic magnetometer for biomedical applications*, *Physics in Medicine & Biology* **58**, 8153 (2013).
- [129] V. Shah and M. V. Romalis, *Spin-exchange relaxation-free magnetometry using elliptically polarized light*, *Physical Review A—Atomic, Molecular, and Optical Physics* **80**, 013416 (2009).
- [130] J. F. Barry, J. M. Schloss, E. Bauch, M. J. Turner, C. A. Hart, L. M. Pham, and R. L. Walsworth, *Sensitivity optimization for nv-diamond magnetometry*, *Reviews of Modern Physics* **92**, 015004 (2020).
- [131] K. Herb, L. A. Völker, J. M. Abendroth, N. Meinhardt, L. van Schie, P. Gambardella, and C. L. Degen, *Quantum magnetometry of transient signals with a time resolution of 1.1 nanoseconds*, *Nature Communications* **16**, 822 (2025).
- [132] B. Fortman, L. Mugica-Sanchez, N. Tischler, C. Selco, Y. Hang, K. Holczer, and S. Takahashi, *Electron–electron double resonance detected*

- nmr spectroscopy using ensemble nv centers at 230 ghz and 8.3 t*, *Journal of Applied Physics* **130**, 10.1063/5.0066759 (2021).
- [133] M. A. Whittington, R. D. Traub, and N. E. Adams, *A future for neuronal oscillation research*, *Brain and neuroscience advances* **2**, 2398212818794827 (2018).
- [134] N. A. Pelot, C. E. Behrend, and W. M. Grill, *Modeling the response of small myelinated axons in a compound nerve to kilohertz frequency signals*, *Journal of neural engineering* **14**, 046022 (2017).
- [135] H. Nury, F. Poitevin, C. V. Renterghem, J.-P. Changeux, P.-J. Corringer, M. Delarue, and M. Baaden, *One-microsecond molecular dynamics simulation of channel gating in a nicotinic receptor homologue*, *Proceedings of the National Academy of Sciences* **107**, 6275 (2010), <https://www.pnas.org/doi/pdf/10.1073/pnas.1001832107>
- [136] M. Brázdil, G. A. Worrell, V. Trávníček, J. Curot, M. Pail, M. Służewska-Niedźwiedź, R. Roman, F. Plešinger, E. Barbeau, M. Kucewicz, *et al.*, *Ultra fast oscillations in the human brain and their functional significance*, *medRxiv*, 2023 (2023).
- [137] B. Hille, *Ionic channels in excitable membranes. current problems and biophysical approaches*, *Biophysical journal* **22**, 283 (1978).
- [138] J. C. Mankins, *Technology readiness assessments: A retrospective*, *Acta Astronautica* **65**, 1216 (2009).
- [139] R. Santagati, A. Aspuru-Guzik, R. Babbush, M. Degroote, L. González, E. Kyoseva, N. Moll, M. Opiel, R. M. Parrish, N. C. Rubin, *et al.*, *Drug design on quantum computers*, *Nature Physics* **20**, 549 (2024).
- [140] N. S. Blunt, J. Camps, O. Crawford, R. Izsák, S. Leontica, A. Mirani, A. E. Moylett, S. A. Scivier, C. Sunderhauf, P. Schopf, *et al.*, *Perspective on the current state-of-the-art of quantum computing for drug discovery applications*, *Journal of Chemical Theory and Computation* **18**, 7001 (2022).
- [141] D. R. Baselt, G. U. Lee, M. Natesan, S. W. Metzger, P. E. Sheehan, and R. J. Colton, *A biosensor based on magnetoresistance technology*, *Biosensors and Bioelectronics* **13**, 731 (1998).
- [142] S. J. Osterfeld, H. Yu, R. S. Gaster, S. Caramuta, L. Xu, S.-J. Han, D. A. Hall, R. J. Wilson, S. Sun, R. L. White, *et al.*, *Multiplex protein assays based on real-time magnetic nanotag sensing*, *Proceedings of the National Academy of Sciences* **105**, 20637 (2008).
- [143] J. Luo, Z. Xu, Z. Jin, M. Wang, X. Cai, and J. Chen, *Development and comprehensive evaluation of TMR sensor-based magnetodes*, *ACS Applied Materials & Interfaces* **16**, 31677 (2024).
- [144] C. Ghemes, O.-G. Dragos-Pinzaru, M. Tibu, M. Lostun, N. Lupu, and H. Chiriac, *Tunnel magnetoresistance-based sensor for biomedical application: Proof-of-concept*, *Coatings* **13**, 10.3390/coatings13020227 (2023).
- [145] W. C. W. Chan and S. Nie, *Quantum dot bioconjugates for ultrasensitive nonisotopic detection*, *Science* **281**, 2016 (1998).
- [146] X. Gao, Y. Cui, R. M. Levenson, L. W. Chung, and S. Nie, *In vivo cancer targeting and imaging with semiconductor quantum dots*, *Nature Biotechnology* **22**, 969 (2004).
- [147] Y. Tang, Q. Zhang, H. Yuan, X. Wang, and L. Xu, *Recent applications and challenges of inorganic nanomaterial-based biosensing devices for detecting nucleic acid biomarkers*, *Advanced Sensor and Energy Materials* 10.1016/j.asems.2025.100136 (2025).
- [148] A. Nakajima, *Application of single-electron transistor to biomolecule and ion sensors*, *Applied Sciences* **6**, 10.3390/app6040094 (2016).
- [149] A. Nakajima, T. Kudo, and S. Furuse, *Biomolecule detection based on Si single-electron transistors for practical use*, *Applied Physics Letters* **103**, 043702 (2013).
- [150] S. Ashoori, M. Naderpour, M. M. Ghezelayagh, R. M. Zadeh, and F. Raissi, *Ultrasensitive bio-detection using single-electron effect*, *Talanta* **224**, 121769 (2021).

Supplementary Material for “Generations of Quantum BioMedical Sensors”

CONTENTS

I. Introduction	1
II. Related Work	2
III. Quantum Medical Sensor Generations	3
IV. Cross-Cutting Considerations	11
Bandwidth Matching and Neural Signal Hierarchy	11
Bridging Clinical Bottlenecks and Technological Maturity	12
V. Conclusion	14
A. Quantum Sensor Timeline Table	20

B. First-Generation Quantum Medical Sensor	20
1. Magnetoresistive biosensors (GMR/TMR)	20
2. Quantum Dots and SET	20
C. Supplementary Sensor Platform Specifications and Readiness Assessment	21

A: Quantum Sensor Timeline Table

Table IV. Representative milestones and reported sensitivities for traditional and quantum biomedical sensors. Values are approximate and normalized for conceptual comparison in Fig. 1.

Year	Technology / Modality	Representative Reference / Device	Physical Principle	Reported Sensitivity	Generation Mapping
1990s	MRI (High-field, 3 T)	Siemens MAGNETOM	Nuclear spin resonance (ensemble)	$\sim 10^{-9}$ T Hz $^{-1/2}$	Classical
2000	EEG	Standard 64-channel system	Cortical electric potential	$\sim 10^{-6}$ V Hz $^{-1/2}$	Classical
2003	SERF atomic magnetometer	Romalis group (Princeton)	Spin-exchange relaxation-free vapor	$\sim 10^{-15}$ T Hz $^{-1/2}$ (fT)	1st Gen
2008	NV-center ODMR in diamond	Taylor et al. (Harvard/MIT)	Electronic spin resonance (ODMR)	$\sim 10^{-9}$ T Hz $^{-1/2}$ (nT)	2nd Gen
2013	Nanoscale NV-NMR	Staudacher et al. / Mamin et al.	Single-spin NMR via NV readout	$\sim 10^{-9}$ T Hz $^{-1/2}$ (nT)	2nd Gen
2015	Sub-pT NV-diamond magnetometer	Wolf et al. (Stuttgart)	Flux-concentrator-enhanced NV ensemble	$\sim 10^{-12}$ T Hz $^{-1/2}$ (pT)	2nd Gen
2016	Spin-squeezed atomic sensor	Hosten et al. (Stanford)	Entanglement-enhanced atom interferometry	~ 20 dB below SQL	3rd Gen
2020	NV ensemble magnetometry (review)	Barry et al. (MIT/Harvard)	Optimized ensemble NV readout	$\sim 10^{-12}$ T Hz $^{-1/2}$ (pT)	2nd-3rd Gen
2023-2025	Quantum-AI hybrid biosensor (prototypes)	Multiple groups (conceptual)	Adaptive sensing / ML feedback	— (conceptual)	4th Gen

B: First-Generation Quantum Medical Sensor

1. Magnetoresistive biosensors (GMR/TMR)

Magnetoresistive biosensors provide a paradigmatic example of first-generation quantum sensing in biomedical applications, where discrete spin-dependent electronic states are exploited for robust signal transduction under ambient conditions. Giant magnetoresistance sensors were first demonstrated as biosensing platforms by Baselt and colleagues, who showed that magnetically labeled DNA hybridization and protein binding events could be detected through resistance changes induced by spin-dependent scattering [141]. Building on this principle, Osterfeld and colleagues developed high-density GMR nanosensor arrays capable of real-time kinetic analysis across multiple protein interactions simultaneously, enabling multiplexed diagnostics and lab-on-chip integration at clinically relevant scales [142]. Tunnel magnetoresistance sensors extend this paradigm by exploiting spin-dependent tunneling through thin insulating barriers, yielding substantially enhanced sensitivity. Recent implementations have integrated TMR sensors into needle-shaped magnetorodes for minimally invasive neurophysiological measurements, achieving sub-nanotesla sensitivity sufficient to resolve magnetic fields generated by individual neuronal action potentials [143]. Complementary studies have demonstrated TMR-based detection of magnetic nanoparticles embedded within tissue phantoms, with direct relevance to magnetic hyperthermia monitoring where accurate spatial localization of therapeutic agents is essential [144]. Together, these results highlight the scalability and clinical relevance of magnetoresistive platforms for point-of-care diagnostics and continuous physiological monitoring.

2. Quantum Dots and SET

Quantum dots and single-electron devices constitute a complementary class of first-generation quantum sensors operating at the nanoscale, where quantization of electronic states enables ultrasensitive molecular detection. Quantum dots have become indispensable tools for fluorescence-based biomedical imaging due to their size-tunable emission spectra and exceptional photostability. The seminal work by Chan and Nie demonstrated that bioconjugated quantum dots could serve as robust probes for cancer biomarker detection, overcoming the

photobleaching limitations of conventional organic fluorophores [145]. Subsequent in vivo studies by Gao and colleagues showed that peptide-functionalized near-infrared quantum dots can selectively accumulate in tumor tissue through receptor-mediated pathways, enabling high-contrast molecular imaging in living systems [146]. More recent reviews have emphasized the integration of quantum dots into hybrid electrical and optical biosensing architectures, particularly for nucleic acid detection where sensitivity and miniaturization are critical [147].

Single-electron transistors offer an alternative route to quantum-enabled biosensing by exploiting charge quantization and Coulomb blockade effects. While early devices required cryogenic operation, advances in silicon nanofabrication have enabled room-temperature biosensors based on multi-island architectures fabricated on silicon-on-insulator substrates [148]. These devices exhibit exceptional charge sensitivity, enabling detection of biomolecular interactions such as streptavidin binding at picomolar concentrations and immunodetection of prostate-specific antigen at clinically relevant thresholds [149]. A macroscopic implementation using porous silicon Schottky junctions further demonstrated that single-electron effects can be preserved across centimeter-scale areas, opening pathways toward low-cost, large-area biosensor arrays suitable for clinical deployment [150]. When integrated with microfluidic and organ-on-chip platforms, these nanoscale quantum sensors offer promising routes toward real-time monitoring of cellular responses and personalized therapeutic screening.

C: Supplementary Sensor Platform Specifications and Readiness Assessment

Table V. Dual-axis cross-platform comparison: physics performance versus translational readiness for representative quantum and conventional biomedical sensing platforms. T_{op} : sensor operating temperature; SWaP-C: size, weight, power, and cost. Gen. column: quantum-technology generation (1st–4th); “—” denotes a classical/conventional platform.

Platform	Gen.	Sensitivity	Bandwidth	Spatial Res.	T_{op} (K)	Sensor-Sample Dist.	Shielding Req.	SWaP-C	Biocompat.	Reg. Path
MRI/fMRI	1–2	$\sim 1\text{--}10 \text{ fT}/\sqrt{\text{Hz}}^\dagger$	MHz (RF)	0.5–2 mm	~ 4 (SC)	5 mm–2 cm	Faraday cage	>\$1 M, tons, >50 kW	External (Gd toxic.)	Cleared (II)
PET/CT	—	Picomolar (mol.)	— (static)	4–5 mm	RT	External ring	None (mag.)	>\$1 M, cyclotron	Ionizing rad.	Cleared (II)
EEG	—	$\sim \mu\text{V}$ (potential)	DC–hundreds Hz	10–25 mm	RT	Scalp contact	None	<\$50 k, portable	Skin contact	Cleared (II)
SQUID-MEG	2nd	$2\text{--}5 \text{ fT}/\sqrt{\text{Hz}}$	DC– ~ 1 kHz	5–10 mm	4.2 (LHe)	2–3 cm (dewar)	Multi-layer MSR	\$2–4 M, >400 kg	External	510(k)
OPM-MEG (SERF)	2nd	$7\text{--}15 \text{ fT}/\sqrt{\text{Hz}}$	DC–200 Hz	3–5 mm	423–473	3–6 mm	MSR + nulling	\$50–200 k, wearable	Skin (insul.)	510(k) pred.
NV diamond (ens.)	1–2	1– $10 \text{ nT}/\sqrt{\text{Hz}}$; $\sim \text{pT}$ pulsed	kHz–GHz	$\sim 10 \mu\text{m}$ (WF); nm	288–333	<1 mm– $10 \mu\text{m}$	None	<\$10 k; miniature	Diamond (inert)	De Novo
FND (nano-diamond)	1st	Single-spin	MHz (relax.)	nm (intracell.)	RT	Zero	None	Minimal	Debated	De Novo
Quantum dots	1st	Molecular (fluor.)	— (steady)	~ 10 nm	RT	Zero (label)	None	Low cost	Cd: toxic; C: good	Material-dep.
Hyperpol. ^{13}C MRI	1→2	$>10^4 \times$ enh.	MHz (MRI)	$\sim \text{mm}$	~ 4 + RT	cm (deep)	MRI built-in	Large: MRI + pol.	No radiation	510(k) ext.
Rydberg atom	2nd	$\text{nV}/\text{cm}/\sqrt{\text{Hz}}$	GHz–THz	$\sim \text{mm}$	298–353	cm (ext.) *	Vacuum cell	Medium, optical	Incompat.	Unclear
Entangled NV pairs	3rd	~ 5 dB > SQL	kHz	<100 nm	RT	<100 nm	None	Lab-scale	Same as NV	Long-term
Spin-squeezed vapor	3rd	~ 2 dB > SQL	DC–kHz	mm–cm	423–473	mm–cm	MSR	OPM + ent.	Same as OPM	Long-term
Distributed QSN	4th	Heisenberg $1/N$	Adaptive	Multi-node	Heterog.	Cross-organ	TBD	QP + transd.	TBD	>10 yr

[†]Surface coil noise-limited sensitivity at clinical field strengths (1.5–3 T).

*Rydberg electrometry achieves 100–500 m detection range for RF fields; for biomedical proximity sensing the practical sensor-sample distance is on the cm scale.

Table VI. Key bottlenecks of existing medical detection devices and corresponding quantum sensing breakthrough directions. For each established clinical modality, the table identifies core limitations, their physical origins, and specific quantum sensor platforms that address each bottleneck.

Existing Device	Core Strengths	Key Bottlenecks / Unmet Needs	Physical Origin of Bottleneck	Quantum Sensor Breakthrough Direction
MRI (1.5–7 T)	Deep tissue; soft-tissue contrast; no ionizing radiation; multi-sequence	(i) Scan 20–60 min, immobility; (ii) fMRI BOLD delay ~ 5 s; (iii) thermal polarization low ($\sim 10^{-5}$); (iv) Gd nephrotoxicity; (v) $> \$1$ M, LHe-dep.; (vi) implant contraindications	Thermal spin polarization very low; BOLD is indirect proxy; SC magnet needs 4 K; SAR limits	Hyperpol. ^{13}C : $> 10^4 \times$ signal \rightarrow metabolic imaging; OPM \rightarrow LHe-free MRI; NV nanoscale NMR; quantum phase estimation \rightarrow accelerated acquisition
PET (FDG)	Picomolar sensitivity; whole-body metabolic; tumor staging gold standard	(i) Ionizing radiation (pediatric); (ii) 4–5 mm resolution; (iii) cyclotron needed; (iv) short tracer half-life; (v) low early-stage sensitivity; (vi) inflammation false positives	e^+ annihilation \rightarrow 511 keV γ \rightarrow inherent radiation; detector geometry; half-life fixed	QD \rightarrow radiation-free labeling; NV relaxometry \rightarrow immunomagnetic; hyperpol. MRI \rightarrow replace some PET; quantum-enhanced photoacoustic
CT	Fast (< 1 min); high spatial resolution; bone/lung; emergency gold standard	(i) Ionizing radiation (cancer risk); (ii) poor soft-tissue contrast; (iii) no metabolic info; (iv) iodine contrast toxicity	X-ray absorption \rightarrow good for bone/air, poor soft tissue; ionizing radiation inherent	Quantum illumination \rightarrow low-dose high-contrast (theoretical); entanglement-enhanced tomography \rightarrow reduced photon requirement
EEG	ms temporal; low cost ($< \$50$ k); non-portable; non-invasive	(i) Poor spatial resolution (cm); (ii) skull distortion (error 25 mm); (iii) EMG/EOG artifacts; (iv) low deep-source sensitivity; (v) no psychiatric biomarker	Skull \rightarrow potential distortion; superposition \rightarrow ill-posed inverse problem	MEG (SQUID/OPM) \rightarrow B unaffected by skull; wearable OPM-MEG; OPM+EEG \rightarrow super-additive source model
SQUID-MEG	fT sensitivity; ms temporal; mm localization; epilepsy gold standard	(i) LHe cryogenics \rightarrow extreme cost; (ii) rigid helmet; (iii) ~ 200 units globally; (iv) 2–3 cm standoff; (v) He volatility $> 400\%$	Josephson junctions need < 4.2 K \rightarrow LHe dewar \rightarrow fixed standoff; He non-renewable	OPM: LHe-free \rightarrow wearable \rightarrow 3–5 \times gain; high- T_c SQUID; NV arrays (long-term)
Tumor biomarkers (PSA, CEA, etc.)	Blood test; simple, low cost, mass screening	(i) Low early-stage sensitivity; (ii) poor specificity; (iii) tumor heterogeneity; (iv) healthy-cell background; (v) ctDNA: 7% Stage I lung	Small tumors release minimal markers; concentration in physiological noise; single-analyte is low-dimensional	SET/QD \rightarrow single-molecule LOD; NV relaxometry \rightarrow wash-free immunoassay; quantum ML \rightarrow pattern recognition; multiplexed quantum arrays